



HAL
open science

Finite element method for stability and free vibration analyses of non-prismatic thin-walled beams

M. Soltani, B. Asgarian, F. Mohri

► **To cite this version:**

M. Soltani, B. Asgarian, F. Mohri. Finite element method for stability and free vibration analyses of non-prismatic thin-walled beams. *Thin-Walled Structures*, 2014, 82, pp.245-261. 10.1016/j.tws.2014.04.012 . hal-01503886

HAL Id: hal-01503886

<https://hal.univ-lorraine.fr/hal-01503886>

Submitted on 23 Jul 2024

HAL is a multi-disciplinary open access archive for the deposit and dissemination of scientific research documents, whether they are published or not. The documents may come from teaching and research institutions in France or abroad, or from public or private research centers.

L'archive ouverte pluridisciplinaire **HAL**, est destinée au dépôt et à la diffusion de documents scientifiques de niveau recherche, publiés ou non, émanant des établissements d'enseignement et de recherche français ou étrangers, des laboratoires publics ou privés.



Distributed under a Creative Commons Attribution - NonCommercial 4.0 International License

Finite element method for stability and free vibration analyses of non-prismatic thin-walled beams

M. Soltani ^{a,*}, B. Asgarian ^a, F. Mohri ^b

^a *K.N.Toosi University of Technology, Tehran, Iran*

^b *Université de Lorraine, Laboratoire d'Etude des Microstructures et de Mécanique des Matériaux (LEM3), CNRS UMR 7239, Metz, France*

In this paper, a numerical method is presented for the free vibration and stability analyses of tapered thin-walled beams with arbitrary open cross sections. The proposed method takes the flexural–torsional coupling effect of tapered thin-walled beams with arbitrary open cross sections into account. The total potential energy is derived for an elastic behavior from the strain energy, the kinetic energy and work of the loads applied on the cross section contour. Free vibration is considered in the presence of harmonic excitations. The effects of the initial stresses and load eccentricities are also considered in stability analysis. The governing equilibrium equations, motion equations and the associated boundary conditions are derived from the stationary condition. As in the presence of tapering, stiffness quantities are not constant; therefore, the power series approximation is used to solve the fourth-order differential equations. Displacement components and cross-section properties are expanded in terms of power series of a known degree. Then, the shape functions are obtained by deriving the deformation shape of tapered thin-walled member as power series form. Finally, stiffness and mass matrices are carried out by means of the principle of virtual work along the member's axis. In order to measure the accuracy and check the validity of this method, the natural frequencies and buckling loads of non-prismatic thin-walled beams with web and flange tapering and various boundary conditions are obtained and compared to the results of finite element analysis using Ansys software and those of other available numerical and analytical ones. It can be seen that the results of present study are in a good agreement with other available theoretical and analytical methods.

1. Introduction

The use of thin walled beams with open variable cross sections has been increasing in steel structures due to their ability to utilize structural material more efficiently and optimize the distribution of weight. With the development of manufacturing process, tapered beams are now adopted with other materials such as wood and concrete. However, prediction of the flexural–torsional buckling loads and vibration of thin walled beams with arbitrary cross-section is complex because of coupling of torsion and bending. The task seems to be more complicated in the presence of non-prismatic thin walled beams where the cross section properties are not constant. The accurate prediction of the buckling load and natural frequencies is one of the important points in the design of thin-walled structures. Meanwhile correct evaluation of stability and free vibration of non-prismatic thin-walled beam with non-symmetric cross-section are of interest to many researchers.

The Timoshenko and Vlasov models [1,2] constitute a powerful background of the rich extensive literature on the elastic flexural–torsional buckling behavior of thin walled beams. Chen, Liu and Bazant, Cedolin evaluated buckling loads either by closed-form solutions of the fourth-order differential equations governing the twisting and bending of the thin-walled beams or by using of complementary energy principle [3,4]. However, these studies are mainly focused on the stability analysis of uniform cross-section beams. Different numerical methods as finite element methods have been developed by many researchers in the case of stability and vibration analyses of prismatic thin walled beams with mono symmetric or arbitrary cross section shapes [5–21]. Most of these studies have been concerned on the stability and vibration analyses of thin-walled beams with uniform cross sections. However, in the last decades, the thin-walled with variable cross sections have been used in different steel constructions; therefore, studying their vibration and stability behavior has gained more attention by many authors [22–36]. The investigations of elastic flexural, lateral-torsional buckling load and natural frequency of tapered thin-walled with the recourse to finite element method in the validation process has been attracted by many researchers.

* Corresponding author. Tel.: +98 21 88779623; fax: +98 21 88779476.
E-mail address: msoltani2@yahoo.com (M. Soltani).

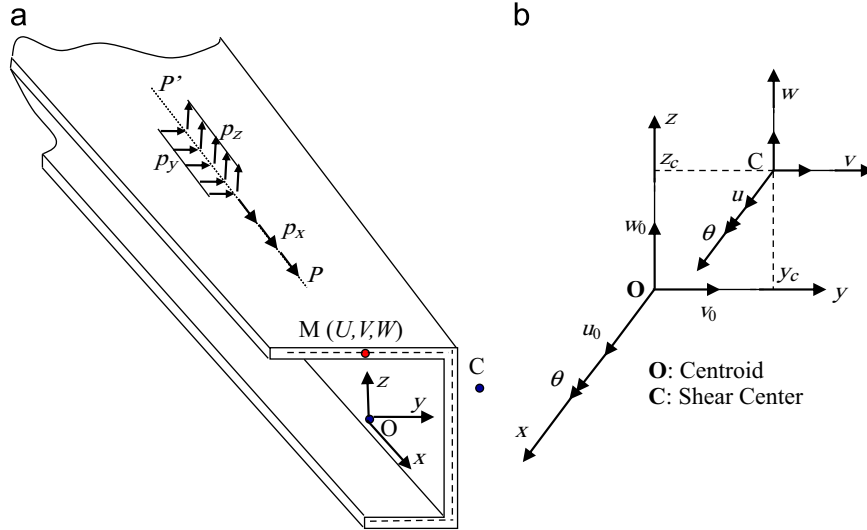


Fig. 1. (a) Thin-walled beam with non-symmetric cross-section and (b) coordinate system and notation for displacement parameters of the non-prismatic beam.

Among the first investigations on this topic, the most important ones are the study of Brown [22] who used shell elements in mesh process of tapered I beams and carried out their buckling loads accordingly. This work was followed by the studies of Yang [23] who used the updated Lagrangian approach to formulate a finite element model for geometrical non-linear analysis. Pasquino [24] used a variational approach to derive the Euler-Lagrange equations to evaluate the buckling loads of non-prismatic thin-walled beams with arbitrary cross-section. A 3D beam finite element model for large torsion context applied to the case of doubly symmetric tapered cross-sections was developed by Ronagh [25,26] in which effects of non-linear terms such as flexural-torsional coupling in the presence of cubic terms of torsion angle were considered. Chen [27] obtained the motion equations governing of non-prismatic thin-walled beams with arbitrary cross-sections by using Hamilton's principle. A finite element approach was introduced by Kim [28] to investigate the linear stability and free vibration behavior of doubly symmetric I tapered thin-walled beam. Li [29] used the Chebyshev polynomial method to solve the equilibrium differential equation of tapered beams under constant axial load and by considering the effect of shear deformation.

The elastic and geometric stiffness matrices of the non-uniform beam element with I section subjected to torsional load is determined by Yau [30]. In the mentioned study, the effects of the non-uniform torsions and the second-order of warping torsions are pondered. Lei [31] established beam strain energy and equilibrium equations considering deformation compatibilities of two the flanges and web of the I-section and investigated the linear stability behavior of the tapered beams. Improved solutions were obtained. More recently, based on the Rayleigh-Ritz method combined with shell element, a general variational formulation to analyze the lateral-torsional buckling behavior of simply supported and cantilever tapered thin-walled beams with singly symmetric cross-sections was presented by Andrade [32-34]. Effects of load position were also modeled in these studies. The lateral stability of thin-walled tapered beams with singly symmetric I cross-sections by means of the power series method was investigated by Asgarian [35]. The previous method has been extended to stability and free vibration behavior of tapered beams with non-symmetric cross-sections and arbitrary boundary conditions using power series expansions by Soltani [36]. Most of the previous works devoted to tapered beams have been limited to doubly or singly symmetric cross-sections in both stability and vibration analyses.

In the present paper, power series method is combined with a finite element approach and applied to tapered beams with arbitrary cross sections. After discretization steps, the stiffness and mass matrices needed in stability and free vibration analyses are determined for non-prismatic thin-walled beams subjected to constant eccentric axial and variable bending loads. The contents of this study are summarized as follows:

1. The equations of motion are derived from the energy principle of the thin-walled beam subjected to bending and axial loads. Load positions on the cross section contour are also taken into account.
2. The power series expansions are used to facilitate the solution of the fourth-order differential equation of equilibrium of non-prismatic thin-walled member with variable coefficients. In this regard, it is assumed that the functions which describe the beam's variable parameters such as: flexural and warping rigidities, density and loads are expanded into power series form. The expressions of shape function are also determined based on aforementioned method.
3. The terms of stiffness and mass matrices are derived by means of the shape functions resulting from its nodal displacements and the principle of virtual work along the beam axis. The critical buckling loads and natural frequencies are also obtained by solving the eigenvalue problem.

After presenting above items, several numerical examples are presented in order to measure the accuracy and validity of the proposed method. The results are also compared with other available results. The present method has many advantages including efficiency, accuracy and simplicity compared to more complicated numerical methods. The main advantage of this method is its simplicities in which for stability and vibration analyses of structure, only geometry and material properties of the members need to be defined.

2. Derivation of equilibrium and motion equations for buckling and free vibration

2.1. Kinematic

A non-prismatic thin-walled beam with arbitrary cross-section as shown in Fig. 1a is considered. It is assumed that the beam is made from homogenous and isotropic material and the length of

the member is large enough compared to its cross-section dimension. Therefore, the shear deformation is negligible and small displacement is considered. In the present study, the beam is subjected to arbitrary distributed forces p_x , p_y and p_z in structural domain in the x , y and z direction, respectively, along a line (PP') on the section contour (Fig. 1a). The shear point C is known by its coordinates (y_c, z_c) in the reference fixed in centroid O . Fig. 1b shows displacement parameters of thin-walled beams defined at the non-symmetric cross-section with reference to centroid or shear points, in which the x , y and z are the cross-section center principal axes. U , V and W are the 3D displacement components of a point on the section contour. θ is the torsion angle. Under these conditions, the three displacement components of point M on the wall contour can be expressed as function of those of the shear center C [36] as follows:

$$U(x, y, z, t) = u_0(x, t) - y \frac{\partial(v(x, t) + z_c(x)\theta(x, t))}{\partial x} - z \frac{\partial(w(x, t) - y_c(x)\theta(x, t))}{\partial x} - \phi(y, z) \frac{\partial\theta(x, t)}{\partial x} \quad (1)$$

$$V(x, y, z, t) = v(x, t) - (z - z_c(x))\theta(x, t) \quad (2)$$

$$W(x, y, z, t) = w(x, t) + (y - y_c(x))\theta(x, t) \quad (3)$$

In these equations, U is the axial displacement at the centroid. The displacement components V and W represent lateral and vertical displacements (in direction the y and z). The term $\phi(y, z)$ signifies a cross-section variable called the warping function, which can be defined based on Saint-Venant's torsion theory. θ is twisting angle.

The Green's strain tensor components which incorporate large displacements and include linear and non-linear parts of strain are given by:

$$\varepsilon_{ij} = \frac{1}{2} \left(\frac{\partial U_i}{\partial x_j} + \frac{\partial U_j}{\partial x_i} \right) + \frac{1}{2} \left(\frac{\partial U_k}{\partial x_i} \frac{\partial U_k}{\partial x_j} \right) = \varepsilon_{ij}^l + \varepsilon_{ij}^* \quad \text{where } i, j, k = x, y, z \quad (4a)$$

ε_{ij}^l denotes the linear and ε_{ij}^* the quadratic non-linear parts of strain. In the case of thin-walled beams, the components of the strain tensor are reduced to the following ones:

$$\varepsilon_{xx} \approx U' + \frac{1}{2}(V'^2 + W'^2) = \varepsilon_{xx}^l + \varepsilon_{xx}^* \quad (4b)$$

$$\varepsilon_{xy} = \frac{1}{2} \left(\frac{\partial U}{\partial y} + \frac{\partial V}{\partial x} \right) + \frac{1}{2} \left(\frac{\partial V}{\partial x} \frac{\partial V}{\partial y} + \frac{\partial W}{\partial x} \frac{\partial W}{\partial y} \right) = \varepsilon_{xy}^l + \varepsilon_{xy}^* \quad (4c)$$

$$\varepsilon_{xz} = \frac{1}{2} \left(\frac{\partial U}{\partial z} + \frac{\partial W}{\partial x} \right) + \frac{1}{2} \left(\frac{\partial V}{\partial x} \frac{\partial V}{\partial z} + \frac{\partial W}{\partial x} \frac{\partial W}{\partial z} \right) = \varepsilon_{xz}^l + \varepsilon_{xz}^* \quad (4d)$$

Using relationships (1-3) and taking into account for tapering, the linear and the quadratic non-linear parts of strain-displacement are as following:

$$\varepsilon_{xx}^l = u_0' - y(v'' + z_c \theta'' + z_c' \theta' + 2z_c' \theta') - z(w'' - y_c \theta'' - y_c' \theta' - 2y_c' \theta') - \phi \theta'' \quad (4e)$$

$$\gamma_{xy}^l = 2\varepsilon_{xy}^l = -(z + (\partial\phi/\partial y))\theta' \quad (4f)$$

$$\gamma_{xz}^l = 2\varepsilon_{xz}^l = (y - (\partial\phi/\partial z))\theta'$$

$$\varepsilon_{xx}^* = \frac{1}{2}[v'^2 + w'^2 + r^2 \theta'^2 + (y_c'^2 + z_c'^2) \theta'^2] - [(y - y_c)y_c' + (z - z_c)z_c']\theta\theta' + (y - y_c)w'\theta' - (z - z_c)v'\theta' - y_c'w'\theta + z_c'v'\theta \quad (4g)$$

$$\gamma_{xy}^* = (w' + \theta'(y - y_c) - \theta y_c')\theta' \quad (4h)$$

$$\gamma_{xz}^* = -(v' + \theta'(z - z_c) + \theta z_c')\theta' \quad (4i)$$

$$\varepsilon_{22} = \varepsilon_{33} = \gamma_{23} = \varepsilon_{22}^* = \varepsilon_{33}^* = \gamma_{23}^* = 0$$

The term r in Eq. (4g) represents the distance of point M to shear center $\sqrt{(y - y_c)^2 + (z - z_c)^2}$.

Then, the stress components for homogenous and isotropic materials are:

$$\sigma_{xx} = E\varepsilon_{xx}, \quad \tau_{xy} = G\gamma_{xy}, \quad \tau_{xz} = G\gamma_{xz}, \quad \sigma_{yy} = \sigma_{zz} = \tau_{yz} = 0, \quad (5)$$

where G and E are shear and Young's modulus.

The most general case of normal and shear stresses associated with axial force N , bending moments M_y and M_z , and shear forces V_y and V_z are considered as:

$$\sigma_{xx}^0 = \frac{N}{A} - \frac{M_y z}{I_y} - \frac{M_z y}{I_z}, \quad \tau_{xy}^0 = \frac{V_y}{A}, \quad \tau_{xz}^0 = \frac{V_z}{A} \quad (6)$$

where τ_{xy}^0 and τ_{xz}^0 represent the mean value of the shear stress and σ_{xx}^0 signifies initial normal stress in the cross section.

2.2. Equations of motion and elastic equilibrium equations

The equations of motion for non-prismatic thin-walled beam are derived by variation of total potential energy which is:

$$\delta(U_I + U_0 + U_M - W) = 0 \quad (7)$$

In the last formulation, δ denotes a virtual variation. U_I and U_0 are the elastic strain energy and the strain energy due to effects of the initial stresses, U_M the kinetic energy under harmonic forces, and W the external load work. Their relationships for each term of the total potential energy are developed separately in the following:

$$\delta U_I = \int_L \int_A (E(\varepsilon_{xx}^l \delta \varepsilon_{xx}^l) + G(\gamma_{xy}^l \delta \gamma_{xy}^l) + G(\gamma_{xz}^l \delta \gamma_{xz}^l)) dA dx \quad (8)$$

$$\delta U_0 = \int_L \int_A (\sigma_{xx}^0 \delta \varepsilon_{xx}^* + \tau_{xy}^0 \delta \gamma_{xy}^* + \tau_{xz}^0 \delta \gamma_{xz}^*) dA dx \quad (9)$$

$$\delta U_M = \omega^2 \int_L \int_A \rho (U \delta U + W \delta W + V \delta V) dA dx \quad (10)$$

$$\delta W = \int_L (p_x \delta u_p + p_y \delta v_p + p_z \delta w_p) dx \quad (11)$$

In which, L and A denote the element length and the cross-section area, respectively, ρ and ω are the material density and the natural frequency (circular). In Eq. (11), u_p , v_p and w_p are axial, lateral and vertical displacements of point P , respectively. According to kinematics used in reference [18] and by adoption the quadratic approximation, the displacements of the point P are:

$$v_p = v - e_z \theta - e_y \frac{\theta^2}{2}, \quad w_p = w + e_y \theta - e_z \frac{\theta^2}{2} \quad (12a, c)$$

$$u_p = u_0 - y_p v_0' - y_p z_c' \theta' - y_p z_c \theta'' - z_p w_0' + z_p y_c' \theta' + z_p y_c \theta'' - \phi_p \theta'$$

For simplicity, $(e_z = z_p - z_c)$ and $(e_y = y_p - y_c)$ are defined to imply the eccentricities of the applied loads from the shear center C of the cross-section.

Substituting the variation of the strain-displacement relations defined in Eq. (4) and initial stresses (6) into Eqs. (8) through (11), and integration over the cross-section in the context of principal bending and warping axes conditions, the following equations are obtained:

$$\delta U_I = \int_L (EA u_0' \delta u_0' + EI_z v'' \delta v'' + EI_y w'' \delta w'' + EI_\phi \theta'' \delta \theta'' + GJ \theta' \delta \theta') dx + \int_L EI_y (-y_c'^2 \theta'' \delta \theta'' + y_c'^2 \theta \delta \theta + 4y_c' \theta' \delta \theta' - y_c' \theta \delta w'' - y_c' w'' \delta \theta - 2y_c' \theta' \delta w'' - 2y_c' w'' \delta \theta' + 2y_c' y_c' \theta' \delta \theta + 2y_c' y_c' \theta \delta \theta') dx$$

$$\begin{aligned}
& + \int_L EI_z (-z_c^2 \theta'' \delta \theta'' + z_c^2 \theta \delta \theta + 4z_c^2 \theta' \delta \theta' + z_c^2 \theta \delta v'' + z_c^2 v'' \delta \theta \\
& + 2z_c \theta' \delta v'' + 2z_c v'' \delta \theta' + 2z_c z_c' \theta' \delta \theta + 2z_c z_c' \theta \delta \theta') dx \quad (13)
\end{aligned}$$

$$\begin{aligned}
U_0 = & \int_L (N(v' \delta v' + w' \delta w' + r_c^2 \theta' \delta \theta' + z_c^2 \theta \delta \theta \\
& + y_c^2 \theta \delta \theta - (z_c z_c') \theta \delta \theta - (y_c y_c') \theta \delta \theta + z_c \theta' \delta v' \\
& + z_c v' \delta \theta' + z_c v' \delta \theta + z_c \theta \delta v' - y_c \theta' \delta w' \\
& - y_c w' \delta \theta' - y_c' w' \delta \theta - y_c' \theta \delta w') - M_z w' \delta \theta' \\
& - M_z \theta' \delta w' + M_y v' \delta \theta' + M_y \theta' \delta v' - M_z w' \delta \theta \\
& - M_z' \theta \delta w' + M_y' v' \delta \theta + M_y' \theta \delta v' \\
& - (M_z y_c' + M_z' y_c) \theta \delta \theta - (M_y z_c' + M_y' z_c) \theta \delta \theta \\
& - (\beta_y M_z + \beta_z M_y) \theta' \delta \theta') dx \quad (14)
\end{aligned}$$

$$\begin{aligned}
\delta U_M = & \omega^2 \int_L (\rho(Au_0 \delta u_0 + Av \delta v + Aw \delta w + I_x \theta \delta \theta + Az_c v \delta \theta \\
& + Az_c \theta \delta v - Ay_c w \delta \theta - Ay_c \theta \delta w + I_\phi \theta' \delta \theta' - I_y y_c^2 \theta' \delta \theta' - I_z z_c^2 \theta' \delta \theta' \\
& + I_z v' \delta v' + I_y w' \delta w' + I_z z_c^2 \theta \delta \theta + I_y y_c^2 \theta \delta \theta \\
& + z_c' I_z v' \delta \theta + z_c' I_z \theta v' - y_c' I_y w' \delta \theta - y_c' I_y \theta w') dx \quad (15)
\end{aligned}$$

$$\begin{aligned}
\delta W = & \int_L (p_x \delta u_0 + p_y \delta v + p_z \delta w - M_{z0} \delta v' - M_{z0} z_c' \delta \theta - M_{z0} z_c \delta \theta' \\
& - M_{y0} \delta w' + M_{y0} y_c' \delta \theta + M_{y0} y_c \delta \theta' + B_{\phi 0} \delta \theta' + \hat{M}_t \delta \theta - M_t \theta \delta \theta) dx \quad (16)
\end{aligned}$$

In the previous expressions (13)–(16), I_ϕ , I_y and I_z denote warping constant and the second moments of inertia. J_s is the Saint-Venant torsion constant. β_y and β_z are Wagner's coefficients in which the exact formulations of these parameters are presented in Asgarian [35]. $M_{z0} = p_x y_p$, $M_{y0} = p_x z_p$ and $B_{\phi 0} = -p_x \phi_p$ are external bending moments and bimoment. $\hat{M}_t = q_z e_y - q_y e_z$ and $M_t = q_y e_y + q_z e_z$ denote the first and second order torsion moments due to load eccentricities. The following geometrical relations are also used:

$$r_c^2 = \frac{I_y}{A} + \frac{I_z}{A} + y_c^2 + z_c^2, \quad I_s = I_y + I_z + A(y_c^2 + z_c^2) \quad (17a, b)$$

In the case of the constant axial load N applied at the beam supports and according to Eq. (7) with respect to u_0 , v , w and θ , the equations of motion for a non-prismatic thin-walled beam with non-symmetric cross-section are derived as:

$$(EAu_0') + \rho \omega^2 Au_0 = p_x \quad (18)$$

$$\begin{aligned}
& (EI_z v'')'' + (EI_z z_c' \theta'')'' + 2(EI_z z_c' \theta')'' - (M_y \theta)'' \\
& - N(v + z_c \theta)'' + \rho \omega^2 Av + \rho \omega^2 Az_c \theta \\
& - \omega^2 (\rho I_z v')' - \omega^2 (\rho z_c' I_z \theta')' = p_y + (M_{z0})' \quad (19)
\end{aligned}$$

$$\begin{aligned}
& (EI_y w'')'' - (EI_y y_c' \theta'')'' - 2(EI_y y_c' \theta')'' + (M_z \theta)'' - N(w - y_c \theta)'' + \rho \omega^2 Aw \\
& - \rho \omega^2 Ay_c \theta - \omega^2 (\rho I_y w')' + \omega^2 (\rho y_c' I_y \theta')' = p_z + (M_{y0})' \quad (20)
\end{aligned}$$

$$\begin{aligned}
& (EI_\phi \theta'')'' - (GJ \theta')' - 4E(y_c^2 I_y + z_c^2 I_z) \theta' + E(y_c^2 I_y + z_c^2 I_z) \theta(x) \\
& + 2E(y_c' I_y w'')' - 2E(z_c' I_z v'')' - E(y_c' I_y w'') + E(z_c' I_z v'') \\
& - 2E(y_c' z_c' I_y + z_c' z_c' I_z) \theta(x) + M_z w'' - M_y v'' - (M_z y_c' + M_z' y_c) \theta(x) \\
& - (M_y z_c' + M_y' z_c) \theta(x) + ((\beta_z M_y + \beta_y M_z) \theta')' - N(r_c^2 \theta')' \\
& - Nz_c v'' + Ny_c w'' - N(z_c z_c' + y_c y_c') \theta(x) + \rho \omega^2 I_s \theta(x) - \omega^2 (\rho I_\phi \theta')' \\
& + \rho \omega^2 (y_c^2 I_y + z_c^2 I_z) \theta(x) + \rho \omega^2 Az_c(x) v(x) - \rho \omega^2 Ay_c(x) w(x) \\
& + \rho \omega^2 I_z z_c' v' - \rho \omega^2 I_y y_c' w' = \hat{M}_t - M_t \theta(x) + (M_{z0}' z_c - M_{y0}' y_c) - (B_{\phi 0})' \quad (21)
\end{aligned}$$

In what follows, a numerical method based on the power series expansions is adopted for solution of the system of coupled differential equations of motion (18)–(21). According to this technique, all geometric properties of a beam with variable

cross-section, the torsion angle θ , the vertical and the lateral displacements are expanded into power series form. This method was used by different authors to derive the critical buckling loads of the beam column members [37–41] and evaluate the stiffness and mass matrices of thin walled beams [14–16]. Its application to non-prismatic thin-walled stability and free vibration analyses is presented in the following section.

3. Numerical approach

In the last equations, due to presence of tapered elements, all geometric properties including bending and torsional characteristics of the beam cross-section along the member length are variable ($I_z(x)$, $I_y(x)$, $I_\phi(x)$, $I_s(x)$). Moreover, the non-symmetric terms are not constant over the beam's length ($z_c(x)$, $y_c(x)$, $\beta_z(x)$, $\beta_y(x)$). All the applied loads, bending and torsion moments can be arbitrary along the x -axis ($M_z(x)$, $M_y(x)$, $M_{z0}(x)$, $M_t(x)$). For these reasons, all these terms are taken as the following infinite power series form:

$$\begin{aligned}
I_z(x) &= \sum_{i=0}^{\infty} I_{zi} x^i, \quad I_y(x) = \sum_{i=0}^{\infty} I_{yi} x^i, \quad I_\phi(x) = \sum_{i=0}^{\infty} I_{\phi i} x^i, \quad I_s(x) = \sum_{i=0}^{\infty} I_{si} x^i, \\
A(x) &= \sum_{i=0}^{\infty} A_i x^i, \quad z_c(x) = \sum_{i=0}^{\infty} z_{ci} x^i, \quad y_c(x) = \sum_{i=0}^{\infty} y_{ci} x^i, \\
\rho(x) &= \sum_{i=0}^{\infty} \rho_i x^i, \quad \beta_z(x) = \sum_{i=0}^{\infty} \beta_{zi} x^i, \quad \beta_y(x) = \sum_{i=0}^{\infty} \beta_{yi} x^i, \\
p_z(x) &= \sum_{i=0}^{\infty} p_{zi} x^i, \quad p_y(x) = \sum_{i=0}^{\infty} p_{yi} x^i, \quad M_t(x) = \sum_{i=0}^{\infty} M_{ti} x^i \\
\hat{M}_t(x) &= \sum_{i=0}^{\infty} \hat{M}_{ti} x^i, \quad M_z(x) = \sum_{i=0}^{\infty} M_{zi} x^i, \quad M_y(x) = \sum_{i=0}^{\infty} M_{yi} x^i, \\
M_{z0}(x) &= \sum_{i=0}^{\infty} M_{z0i} x^i, \quad M_{y0}(x) = \sum_{i=0}^{\infty} M_{y0i} x^i, \quad B_{\phi 0}(x) = \sum_{i=0}^{\infty} B_{\phi 0i} x^i \quad (22)
\end{aligned}$$

In beam stability and free vibration analyses, the axial equilibrium equation Eq. (17) is uncoupled to flexural-torsional behavior and it has no incidence on analyses. Therefore, in what follows, this equation is not considered. Introducing a non-dimensional variable ($\varepsilon = x/L$), the stability Eqs. (19)–(21) are written in terms of ε as:

$$\begin{aligned}
& \frac{d^2}{d\varepsilon^2} \left[E \sum_{i=0}^{\infty} I_{xi} L^i \varepsilon^i \right] \frac{d^2 v}{d\varepsilon^2} + E \frac{d^2 v}{d\varepsilon^2} \left[\sum_{j=0}^{\infty} \sum_{i=0}^{\infty} (j+1) I_{zj} z_{c_{j+2}} L^{i+j+2} \varepsilon^{i+j} \right] \theta(\varepsilon) \\
& + 2E \frac{d^2}{d\varepsilon^2} \left[\sum_{j=0}^{\infty} \sum_{i=0}^{\infty} (j+1) I_{zj} z_{c_{j+1}} L^{i+j+1} \varepsilon^{i+j} \right] \frac{d\theta}{d\varepsilon} \\
& - (L^2) \frac{d^2}{d\varepsilon^2} \left[\left(\sum_{i=0}^{\infty} M_{yi} L^i \varepsilon^i \right) \theta(\varepsilon) \right] - (L^2) N \frac{d^2}{d\varepsilon^2} v(\varepsilon) + \theta(\varepsilon) \sum_{i=0}^{\infty} z_{ci} L^i \varepsilon^i \\
& + (L^4) \omega^2 \sum_{j=0}^{\infty} \sum_{i=0}^{\infty} \rho_i A_j L^{i+j} \varepsilon^{i+j} \\
& v(\varepsilon) + (L^4) \omega^2 \left(\sum_{m=0}^{\infty} \sum_{j=0}^{\infty} \sum_{i=0}^{\infty} \rho_i A_j z_{c_{m+1}} L^{i+j+m} \varepsilon^{i+j+m} \right) \theta(\varepsilon) \\
& - (L^2) \omega^2 \frac{d}{d\varepsilon} \left[\left(\sum_{j=0}^{\infty} \sum_{i=0}^{\infty} \rho_i I_{zj} L^{i+j} \varepsilon^{i+j} \right) \frac{dv}{d\varepsilon} \right] \\
& - (L^2) \omega^2 \frac{d}{d\varepsilon} \left[\left(\sum_{m=0}^{\infty} \sum_{j=0}^{\infty} \sum_{i=0}^{\infty} (m+1) \rho_i I_{yj} z_{c_{m+1}} L^{i+j+m+1} \varepsilon^{i+j+m} \right) \theta(\varepsilon) \right] \\
& = L^4 \sum_{i=0}^{\infty} p_{yi} L^i \varepsilon^i + L^3 \sum_{i=0}^{\infty} (i+1) M_{z0i+1} L^{i+1} \varepsilon^i \quad (23)
\end{aligned}$$

$$\frac{d^2}{d\varepsilon^2} \left[F \sum_{i=0}^{\infty} I_{yi} L^i \varepsilon^i \right] \frac{d^2 w}{d\varepsilon^2} - E \frac{d^2}{d\varepsilon^2} \left[\sum_{j=0}^{\infty} \sum_{i=0}^{\infty} (j+2)(j+1) I_{yj} y_{c_{j+2}} L^{i+j+2} \varepsilon^{i+j} \right] \theta(\varepsilon)$$

$$\begin{aligned}
& -2E \frac{d^2}{d\varepsilon^2} \left[\sum_{j=0}^{\infty} \sum_{i=0}^{\infty} (j+1) I_{y_i} y_{c_{j+1}} L^{i+j+1} \varepsilon^{i+j} \right] \frac{d\theta}{d\varepsilon} \\
& + (L^2) \frac{d^2}{d\varepsilon^2} \left[\left(\sum_{i=0}^{\infty} M_{z_i} L^i \varepsilon^i \right) \theta(\varepsilon) \right] - (L^2) N \frac{d^2}{d\varepsilon^2} w(\varepsilon) - \theta(\varepsilon) \sum_{i=0}^{\infty} y_{c_i} L^i \varepsilon^i \\
& + (L^4) \omega^2 \sum_{j=0}^{\infty} \sum_{i=0}^{\infty} \rho_i A_j L^{i+j} \varepsilon^{i+j} w(\varepsilon) \\
& - (L^4) \omega^2 \left(\sum_{m=0}^{\infty} \sum_{j=0}^{\infty} \sum_{i=0}^{\infty} \rho_i A_j y_{c_m} L^{i+j+m} \varepsilon^{i+j+m} \right) \theta(\varepsilon) \\
& - (L^2) \omega^2 \frac{d}{d\varepsilon} \left[\left(\sum_{j=0}^{\infty} \sum_{i=0}^{\infty} \rho_i I_{y_j} L^{i+j} \varepsilon^{i+j} \right) \frac{dw}{d\varepsilon} \right] \\
& + (L^2) \omega^2 \frac{d}{d\varepsilon} \left[\left(\sum_{m=0}^{\infty} \sum_{j=0}^{\infty} \sum_{i=0}^{\infty} (m+1) \rho_i I_{y_j} y_{c_{m+1}} L^{i+j+m+1} \varepsilon^{i+j+m} \right) \theta(\varepsilon) \right] \\
& = L^4 \sum_{i=0}^{\infty} p_{z_i} L^i \varepsilon^i + L^3 \sum_{i=0}^{\infty} (i+1) M_{y_{0i+1}} L^{i+1} \varepsilon^i \quad (24)
\end{aligned}$$

$$\begin{aligned}
& \frac{d^2}{d\varepsilon^2} \left[E \sum_{i=0}^{\infty} I_{\phi_i} L^i \varepsilon^i \right] \frac{d^2 \theta}{d\varepsilon^2} - (L^2) \frac{d}{d\varepsilon} \left[G \sum_{i=0}^{\infty} J_i L^i \varepsilon^i \right] \frac{d\theta}{d\varepsilon} \\
& - 4E \frac{d}{d\varepsilon} \left[\left(\sum_{m=0}^{\infty} \sum_{j=0}^{\infty} \sum_{i=0}^{\infty} (j+1)(m+1) (I_{y_i} y_{c_{j+1}} y_{c_{m+1}} + I_{z_i} z_{c_{j+1}} z_{c_{m+1}}) \right. \right. \\
& \left. \left. L^{i+j+m+2} \varepsilon^{i+j+m} \right) \frac{d\theta}{d\varepsilon} \right] + E \sum_{m=0}^{\infty} \sum_{j=0}^{\infty} \sum_{i=0}^{\infty} (j+1)(j+2)(m+1)(m+2) \\
& (I_{y_i} y_{c_{j+2}} y_{c_{m+2}} + I_{z_i} z_{c_{j+2}} z_{c_{m+2}}) L^{i+j+m+4} \varepsilon^{i+j+m} \\
& \theta(\varepsilon) + 2E \frac{d}{d\varepsilon} \left[\left(\sum_{j=0}^{\infty} \sum_{i=0}^{\infty} (j+1) I_{y_i} y_{c_{j+1}} L^{i+j+1} \varepsilon^{i+j} \right) \frac{d^2 w}{d\varepsilon^2} \right] \\
& - \left(\sum_{j=0}^{\infty} \sum_{i=0}^{\infty} (j+1) I_{z_i} z_{c_{j+1}} L^{i+j+1} \varepsilon^{i+j} \right) \frac{d^2 v}{d\varepsilon^2} \\
& - E \left(\sum_{j=0}^{\infty} \sum_{i=0}^{\infty} (j+1)(j+2) I_{y_i} y_{c_{j+2}} L^{i+j+2} \varepsilon^{i+j} \right) \frac{d^2 w}{d\varepsilon^2} \\
& + E \sum_{j=0}^{\infty} \sum_{i=0}^{\infty} (j+1)(j+2) I_{z_i} z_{c_{j+2}} L^{i+j+2} \varepsilon^{i+j} \frac{d^2 v}{d\varepsilon^2} \\
& - 2E \left[\frac{d}{d\varepsilon} \left(\sum_{m=0}^{\infty} \sum_{j=0}^{\infty} \sum_{i=0}^{\infty} (j+1)(m+1)(m+2) (I_{y_i} y_{c_{j+1}} y_{c_{m+2}} \right. \right. \\
& \left. \left. + I_{z_i} z_{c_{j+1}} z_{c_{m+2}}) L^{i+j+m+3} \varepsilon^{i+j+m} \right) \theta(\varepsilon) + (L^2) \sum_{i=0}^{\infty} M_{z_i} L^i \varepsilon^i \right] \left(\frac{d^2 w}{d\varepsilon^2} \right) \\
& - (L^2) \sum_{i=0}^{\infty} M_{y_i} L^i \varepsilon^i \left(\frac{d^2 v}{d\varepsilon^2} \right) - (L^2) \\
& \sum_{j=0}^{\infty} \sum_{i=0}^{\infty} ((j+1)(j+2) M_{z_i} y_{c_{j+2}} + (i+1)(i+2) M_{z_{i+2}} y_{c_j}) L^{i+j+2} \varepsilon^{i+j} \theta(\varepsilon) \\
& - (L^2) \left(\sum_{j=0}^{\infty} \sum_{i=0}^{\infty} ((j+1)(j+2) M_{y_i} z_{c_{j+2}} + (i+1)(i+2) M_{y_{i+2}} z_{c_j}) L^{i+j+2} \varepsilon^{i+j} \right) \\
& \theta(\varepsilon) + (L^2) \frac{d}{d\varepsilon} \left[\left(\sum_{j=0}^{\infty} \sum_{i=0}^{\infty} (M_{y_i} \beta_{z_j} + M_{z_i} \beta_{y_j}) L^{i+j} \varepsilon^{i+j} \right) \frac{d\theta}{d\varepsilon} \right] \\
& - (L^2) N \frac{d}{d\varepsilon} \left[\left(\sum_{i=0}^{\infty} R_{c_i} L^i \varepsilon^i \right) \frac{d\theta}{d\varepsilon} \right] - (L^2) N \sum_{i=0}^{\infty} z_{c_i} L^i \varepsilon^i \frac{d^2 v}{d\varepsilon^2} \\
& + (L^2) N \left(\sum_{i=0}^{\infty} y_{c_i} L^i \varepsilon^i \right) \frac{d^2 w}{d\varepsilon^2} \\
& - (L^2) N \left(\sum_{j=0}^{\infty} \sum_{i=0}^{\infty} (j+1)(j+2) (z_{c_i} z_{c_{j+2}} + y_{c_i} y_{c_{j+2}}) L^{i+j+2} \varepsilon^{i+j} \right) \\
& \theta(\varepsilon) + (L^4) \omega^2 \left(\sum_{j=0}^{\infty} \sum_{i=0}^{\infty} \rho_i I_{s_j} L^{i+j} \varepsilon^{i+j} \right) \theta(\varepsilon) \quad (25)
\end{aligned}$$

$$\begin{aligned}
& - (L^2) \omega^2 \frac{d}{d\varepsilon} \left[\sum_{j=0}^{\infty} \sum_{i=0}^{\infty} \rho_i I_{\phi_j} L^{i+j} \varepsilon^{i+j} \right] \frac{d\theta}{d\varepsilon} \\
& + (L^2) \omega^2 \left(\sum_{n=0}^{\infty} \sum_{m=0}^{\infty} \sum_{j=0}^{\infty} \sum_{i=0}^{\infty} (m+1)(n+1) \rho_i (I_{y_i} y_{c_{m+1}} y_{c_{n+1}} + I_{z_i} z_{c_{m+1}} z_{c_{n+1}}) \right. \\
& \left. L^{i+j+m+n+2} \varepsilon^{i+j+m+n} \right) \theta(\varepsilon) \\
& + (L^4) \omega^2 \left(\sum_{m=0}^{\infty} \sum_{j=0}^{\infty} \sum_{i=0}^{\infty} \rho_i A_j z_{c_m} L^{i+j+m} \varepsilon^{i+j+m} \right) v(\varepsilon) \\
& - (L^4) \omega^2 \left(\sum_{m=0}^{\infty} \sum_{j=0}^{\infty} \sum_{i=0}^{\infty} \rho_i A_j y_{c_m} L^{i+j+m} \varepsilon^{i+j+m} \right) w(\varepsilon) \\
& + (L^2) \omega^2 \left(\sum_{m=0}^{\infty} \sum_{j=0}^{\infty} \sum_{i=0}^{\infty} (m+1) \rho_i I_{z_i} z_{c_{m+1}} L^{i+j+m+1} \varepsilon^{i+j+m} \right) \left(\frac{dv}{d\varepsilon} \right) \\
& - (L^2) \omega^2 \left(\sum_{m=0}^{\infty} \sum_{j=0}^{\infty} \sum_{i=0}^{\infty} (m+1) \rho_i I_{y_i} y_{c_{m+1}} L^{i+j+m+1} \varepsilon^{i+j+m} \right) \left(\frac{dw}{d\varepsilon} \right) \\
& = (L^4) \sum_{i=0}^{\infty} \hat{M}_{t_i} L^i \varepsilon^i - (L^4) \left(\sum_{i=0}^{\infty} M_{t_i} L^i \varepsilon^i \right) \theta(\varepsilon) \\
& + (L^3) \left(\sum_{j=0}^{\infty} \sum_{i=0}^{\infty} (j+1) z_{c_i} M_{z_{0j+1}} L^{i+j+1} \varepsilon^{i+j} - \sum_{j=0}^{\infty} \sum_{i=0}^{\infty} (j+1) y_{c_i} M_{y_{0j+1}} L^{i+j+1} \varepsilon^{i+j} \right) \\
& - (L^3) \sum_{i=0}^{\infty} B_{\phi_{0i+1}} (i+1) L^{i+1} \varepsilon^i
\end{aligned}$$

The general solutions of three displacement parameters $(v(\varepsilon), w(\varepsilon), \theta(\varepsilon))$ are also presented using the following power series:

$$v(\varepsilon) = \sum_{i=0}^{\infty} a_i \varepsilon^i \quad (26)$$

$$w(\varepsilon) = \sum_{i=0}^{\infty} b_i \varepsilon^i \quad (27)$$

$$\theta(\varepsilon) = \sum_{i=0}^{\infty} c_i \varepsilon^i \quad (28)$$

Furthermore, introducing new variables:

$$\begin{aligned}
I_{z_i}^* &= I_{z_i} L^i, & I_{y_i}^* &= I_{y_i} L^i, & I_{\phi_i}^* &= I_{\phi_i} L^i, \\
I_{s_i}^* &= I_{s_i} L^i, & J_i^* &= J_i L^i, & R_{c_i}^* &= R_{c_i} L^i, & A_i^* &= A_i L^i \\
z_{c_i}^* &= z_{c_i} L^i, & y_{c_i}^* &= y_{c_i} L^i, & \rho_i^* &= \rho_i L^i, & \beta_{z_i}^* &= \beta_{z_i} L^i, \\
\beta_{y_i}^* &= \beta_{y_i} L^i, & p_{z_i}^* &= p_{z_i} L^i, & p_{y_i}^* &= p_{y_i} L^i \\
B_{\phi_{0i}}^* &= B_{\phi_{0i}} L^i, & M_{z_i}^* &= M_{z_i} L^i, & M_{y_i}^* &= M_{y_i} L^i, \\
M_{z_{0i}}^* &= M_{z_{0i}} L^i, & M_{y_{0i}}^* &= M_{y_{0i}} L^i, & M_{t_i}^* &= M_{t_i} L^i, & \hat{M}_{t_i}^* &= \hat{M}_{t_i} L^i \quad (29)
\end{aligned}$$

To satisfy Eqs. (23)-(25) for all values of ε , one must have the following recurrence formula for a_{k+4} , b_{k+4} and c_{k+4} :

$$\begin{aligned}
a_{k+4} &= \frac{-1}{EI_{z_0}^* (k+4)(k+3)(k+2)(k+1)} \\
& \left[E \sum_{i=1}^{k+2} I_{z_i}^* a_{k-i+4} (k-i+4)(k-i+3)(k+2)(k+1) \right] \\
& + E \left(\sum_{j=0}^{k+2} \sum_{i=0}^j I_{z_i}^* z_{c_{j-i+2}}^* c_{k-j+2} (j-i+2)(j-i+1)(k+2)(k+1) \right) \\
& + 2E \left(\sum_{j=0}^{k+2} \sum_{i=0}^j I_{z_i}^* z_{c_{j-i+1}}^* c_{k-j+3} (j-i+1)(k-j+3)(k+2)(k+1) \right) \\
& - (L^2) N \left(a_{k+2} (k+1)(k+2) + \sum_{i=0}^{k+2} z_{c_i}^* c_{k-i+2} (k+1)(k+2) \right) \\
& - (L^2) \sum_{i=0}^{k+2} M_{y_i}^* c_{k-i+2} (k+2)(k+1) + (L^4) \omega^2 \sum_{j=0}^k \sum_{i=0}^j \rho_i^* A_{j-i}^* a_{k-j}
\end{aligned}$$

$$\begin{aligned}
& + (L^4)\omega^2 \left(\sum_{m=j}^k \sum_{i=0}^m \sum_{i=0}^j \rho_i^* A_{j-i}^* z_{c_{m-j}}^* c_{k-m} \right) \\
& - (L^2)\omega^2 \left(\sum_{j=0}^{k+1} \sum_{i=0}^j \rho_i^* I_{z_{j-i}}^* a_{k-j+2}(k-j+2)(k+1) \right) \\
& - (L^2)\omega^2 \left(\sum_{m=j}^{k+1} \sum_{i=0}^m \sum_{i=0}^j \rho_i^* I_{z_{j-i}}^* z_{c_{m-j+1}}^* c_{k-j+1}(m-j+1)(k+1) \right) \\
& - (L^4)p_{y_k}^* + (L^3)(k+1)M_{z0_{k+1}}^* \Big] \text{ for } k=0, 1, 2, \dots
\end{aligned} \tag{30}$$

$$\begin{aligned}
& + (L^2) \left(\sum_{i=0}^k M_{z_i}^* b_{k-i+2}(k-i+2)(k-i+1) \right) \\
& - (L^2) \left(\sum_{i=0}^k M_{y_i}^* a_{k-i+2}(k-i+2)(k-i+1) \right) \\
& - (L^2) \left(\sum_{j=0}^k \sum_{i=0}^j (M_{z_i}^* y_{c_{j-i+2}}^* (j-i+1)(j-i+2) + M_{y_{i+2}}^* z_{c_{j-i}}^* (i+1)(i+2)) c_{k-j} \right) \\
& - (L^2) \left(\sum_{j=0}^k \sum_{i=0}^j (M_{y_i}^* z_{c_{j-i+2}}^* (j-i+1)(j-i+2) + M_{z_{i+2}}^* y_{c_{j-i}}^* (i+1)(i+2)) c_{k-j} \right) \\
& + (L^2) \left(\sum_{j=0}^{k+1} \sum_{i=0}^j (M_{y_i}^* \beta_{z_{j-i}}^* + M_{z_i}^* \beta_{y_{j-i}}^*) c_{k-j+2}(k+1)(k-j+2) \right) \\
& - (L^2)N \left(\sum_{i=0}^{k+1} R_{c_i}^* c_{k-i+2}(k-i+2)(k+1) \right)
\end{aligned} \tag{32}$$

$$\begin{aligned}
b_{k+4} &= \frac{-1}{E I_{y_0}^* (k+4)(k+3)(k+2)(k+1)} \\
& \left[E \sum_{i=1}^{k+2} I_{y_i}^* b_{k-i+4}(k-i+4)(k-i+3)(k+2)(k+1) \right. \\
& - E \left(\sum_{j=0}^{k+2} \sum_{i=0}^j I_{y_i}^* y_{c_{j-i+2}}^* c_{k-j+2}(j-i+2)(j-i+1)(k+2)(k+1) \right) \\
& - 2E \left(\sum_{j=0}^{k+2} \sum_{i=0}^j I_{y_i}^* y_{c_{j-i+1}}^* c_{k-j+3}(j-i+1)(k-j+3)(k+2)(k+1) \right) \\
& - (L^2)N \left(b_{k+2}(k+1)(k+2) - \sum_{i=0}^{k+2} y_{c_i}^* c_{k-i+2}(k+1)(k+2) \right) \\
& - (L^2) \sum_{i=0}^{k+2} M_{z_i}^* c_{k-i+2}(k+2)(k+1) + (L^4)\omega^2 \sum_{j=0}^k \sum_{i=0}^j \rho_i^* A_{j-i}^* b_{k-j} \\
& - (L^4)\omega^2 \left(\sum_{m=j}^k \sum_{i=0}^m \sum_{i=0}^j \rho_i^* A_{j-i}^* z_{c_{m-j}}^* c_{k-m} \right) \\
& - (L^2)\omega^2 \left(\sum_{j=0}^{k+1} \sum_{i=0}^j \rho_i^* I_{y_{j-i}}^* b_{k-j+2}(k-j+1)(k+1) \right) \\
& + (L^2)\omega^2 \left(\sum_{m=j}^{k+1} \sum_{i=0}^m \sum_{i=0}^j \rho_i^* I_{y_{j-i}}^* y_{c_{m-j+1}}^* c_{k-j}(m-j+1)(k+1) \right) \\
& - (L^4)p_{z_k}^* - (L^3)(k+1)M_{y0_{k+1}}^* \Big] \text{ for } k=0, 1, 2, \dots
\end{aligned} \tag{31}$$

$$\begin{aligned}
c_{k+4} &= \frac{-1}{E I_{\phi_0}^* (k+4)(k+3)(k+2)(k+1)} \\
& \left[E \sum_{i=1}^{k+2} I_{\phi_i}^* c_{k-i+4}(k-i+4)(k-i+3)(k+2)(k+1) \right. \\
& - (L^2) \sum_{i=0}^{k+1} G_{j_i}^* c_{k-i+2}(k+1)(k-i+2) \\
& - 4E \sum_{m=0}^{k+1} \sum_{j=0}^m \sum_{i=0}^j (I_{y_i}^* y_{c_{j-i+1}}^* y_{c_{m-j+1}}^* + I_{z_i}^* z_{c_{j-i+1}}^* z_{c_{m-j+1}}^*) \\
& c_{k-m+2}(j-i+1)(m-j+1)(k-m+2)(k+1) \\
& + E \left(\sum_{m=0}^k \sum_{j=0}^m \sum_{i=0}^j (I_{y_i}^* y_{c_{j-i+2}}^* y_{c_{m-j+2}}^* + I_{z_i}^* z_{c_{j-i+2}}^* z_{c_{m-j+2}}^*) \right. \\
& c_{k-m}(j-i+1)(j-i+2)(m-j+2)(m-j+1) \\
& + 2E \sum_{j=0}^{k+1} \sum_{i=0}^j (I_{y_i}^* y_{c_{j-i+1}}^* b_{k-j+3} - I_{z_i}^* z_{c_{j-i+1}}^* a_{k-j+3} \\
& (j-i+1)(k-j+2)(k-j+3)(k+1) \\
& - E \sum_{j=0}^k \sum_{i=0}^j (I_{y_i}^* y_{c_{j-i+2}}^* b_{k-j+2} - I_{z_i}^* z_{c_{j-i+2}}^* a_{k-j+2} \\
& (j-i+1)(j-i+2)(k-j+1)(k-j+2) \\
& \left. - 2E \sum_{m=0}^k \sum_{j=0}^{m+1} \sum_{i=0}^j (I_{y_i}^* y_{c_{j-i+1}}^* y_{c_{m-j+3}}^* + I_{z_i}^* z_{c_{j-i+1}}^* z_{c_{m-j+3}}^*) \right. \\
& c_{k-m}(j-i+1)(m-j+3)(m-j+2)(m+1)
\end{aligned}$$

$$\begin{aligned}
& - (L^2)N \sum_{i=0}^k z_{c_i}^* a_{k-i+2}(k-i+1)(k-i+2) \\
& + (L^2)N \left(\sum_{i=0}^k y_{c_i}^* b_{k-i+2}(k-i+1)(k-i+2) \right) \\
& - (L^2)N \left(\sum_{j=0}^k \sum_{i=0}^j (z_{c_i}^* z_{c_{j-i+2}}^* + y_{c_i}^* y_{c_{j-i+2}}^*) c_{k-j}(j-i+1)(j-i+2) \right) \\
& + (L^4)\omega^2 \left(\sum_{j=0}^k \sum_{i=0}^j \rho_i^* I_{s_{j-i}}^* c_{k-j} \right) \\
& - (L^2)\omega^2 \left(\sum_{j=0}^{k+1} \sum_{i=0}^j \rho_i^* I_{\phi_{j-i}}^* c_{k-j+2}(k+1)(k-j+2) \right) \\
& + (L^4)\omega^2 \left(\sum_{m=0}^k \sum_{j=0}^m \sum_{i=0}^j \rho_i^* A_{j-i}^* z_{c_{m-j}}^* a_{k-m} \right) \\
& - (L^4)\omega^2 \left(\sum_{m=0}^k \sum_{j=0}^m \sum_{i=0}^j \rho_i^* A_{j-i}^* y_{c_{m-j}}^* b_{k-m} \right) \\
& + (L^2)\omega^2 \left(\sum_{n=0}^k \sum_{m=0}^n \sum_{j=0}^m \sum_{i=0}^j \rho_i^* (I_{y_{j-i}}^* y_{c_{m-j+1}}^* y_{c_{n-m+1}}^* \right. \\
& + I_{z_{j-i}}^* z_{c_{m-j+1}}^* z_{c_{n-m+1}}^*) c_{k-n}(m-j+1)(n-m+1) \\
& \left. + (L^2)\omega^2 \left(\sum_{m=0}^k \sum_{j=0}^m \sum_{i=0}^j \rho_i^* I_{z_{j-i}}^* z_{c_{m-j+1}}^* a_{k-m+1}(m-j+1)(k-m+1) \right) \right. \\
& - (L^2)\omega^2 \sum_{m=0}^k \sum_{j=0}^m \sum_{i=0}^j \rho_i^* I_{y_{j-i}}^* y_{c_{m-j+1}}^* b_{k-m+1}(m-j+1)(k-m+1) \\
& - (L^4)\hat{M}_{tk}^* + (L^4) \sum_{i=0}^k M_{ti}^* c_{k-i} \\
& - (L^3) \left(\sum_{i=0}^k z_{c_i}^* M_{z0_{k-i+1}}^* (k-i+1) - \sum_{i=0}^k y_{c_i}^* M_{y0_{k-i+1}}^* (k-i+1) \right) \\
& \left. + (L^3)B_{\phi0_{k+1}}^* (k+1) \right] \text{ for } k=0, 1, 2, 3, 4, \dots
\end{aligned}$$

According to the recurrence formulas (30)–(32), the general solution of coupled system of differential Eqs. (19)–(21) can be determined explicitly in terms of the twelve constants (a_0, a_1, a_2, a_3) , (b_0, b_1, b_2, b_3) and (c_0, c_1, c_2, c_3) . Then, the solutions of equilibrium equations can be expressed in the following matrix form:

$$\{C(\varepsilon)\} = [B(\varepsilon)]\{A\} \tag{33}$$

In which

$$\{C(\varepsilon)\} = \begin{Bmatrix} v(\varepsilon) \\ w(\varepsilon) \\ \theta(\varepsilon) \end{Bmatrix}$$

$$\{A\} = \{a_0 \ a_1 \ a_2 \ a_3 \ b_0 \ b_1 \ b_2 \ b_3 \ c_0 \ c_1 \ c_2 \ c_3\}^T$$

$$[B(\varepsilon)] = \begin{bmatrix} v_0(\varepsilon) & v_1(\varepsilon) & v_2(\varepsilon) & v_3(\varepsilon) & v_4(\varepsilon) & v_5(\varepsilon) & v_6(\varepsilon) & v_7(\varepsilon) & v_8(\varepsilon) & v_9(\varepsilon) & v_{10}(\varepsilon) & v_{11}(\varepsilon) \\ w_0(\varepsilon) & w_1(\varepsilon) & w_2(\varepsilon) & w_3(\varepsilon) & w_4(\varepsilon) & w_5(\varepsilon) & w_6(\varepsilon) & w_7(\varepsilon) & w_8(\varepsilon) & w_9(\varepsilon) & w_{10}(\varepsilon) & w_{11}(\varepsilon) \\ \theta_0(\varepsilon) & \theta_1(\varepsilon) & \theta_2(\varepsilon) & \theta_3(\varepsilon) & \theta_4(\varepsilon) & \theta_5(\varepsilon) & \theta_6(\varepsilon) & \theta_7(\varepsilon) & \theta_8(\varepsilon) & \theta_9(\varepsilon) & \theta_{10}(\varepsilon) & \theta_{11}(\varepsilon) \end{bmatrix} \quad (34a-c)$$

In Eq. (33), $\{A\}$ is unknown vector. All terms ($v_i(\varepsilon), w_i(\varepsilon)$ and $\theta_i(\varepsilon)$, $i=0-11$) are derived using MATLAB software [42].

4. Boundary conditions and shape functions

It should be noted that the all undefined coefficients (a_0, a_1, a_2, a_3), (b_0, b_1, b_2, b_3) and (c_0, c_1, c_2, c_3) are functions of the displacements of degree of freedom (DOF) which can be derived by imposing four boundary conditions for each displacement parameter of a single-span beam (two at each end of the beam). Fig. 2 shows the nodal displacements of the beam element in the local coordinate.

Referring to this figure and using local coordinates at $\varepsilon = 0$ and $\varepsilon = 1$, the following boundary conditions must be satisfied:

$$\{D\} = [V]\{A\} \quad (35)$$

Where

$$V = \begin{bmatrix} v_0(0) & v_1(0) & v_2(0) & \dots & v_{11}(0) \\ w_0(0) & w_1(0) & w_2(0) & \dots & w_{11}(0) \\ \theta_0(0) & \theta_1(0) & \theta_2(0) & \dots & \theta_{11}(0) \\ \frac{v_0'(0)}{L} & \frac{v_1'(0)}{L} & \frac{v_2'(0)}{L} & \dots & \frac{v_{11}'(0)}{L} \\ \frac{w_0'(0)}{L} & \frac{w_1'(0)}{L} & \frac{w_2'(0)}{L} & \dots & \frac{w_{11}'(0)}{L} \\ \frac{\theta_0'(0)}{L} & \frac{\theta_1'(0)}{L} & \frac{\theta_2'(0)}{L} & \dots & \frac{\theta_{11}'(0)}{L} \\ v_0(1) & v_1(1) & v_2(1) & \dots & v_{11}(1) \\ w_0(1) & w_1(1) & w_2(1) & \dots & w_{11}(1) \\ \theta_0(1) & \theta_1(1) & \theta_2(1) & \dots & \theta_{11}(1) \\ \frac{v_0'(1)}{L} & \frac{v_1'(1)}{L} & \frac{v_2'(1)}{L} & \dots & \frac{v_{11}'(1)}{L} \\ \frac{w_0'(1)}{L} & \frac{w_1'(1)}{L} & \frac{w_2'(1)}{L} & \dots & \frac{w_{11}'(1)}{L} \\ \frac{\theta_0'(1)}{L} & \frac{\theta_1'(1)}{L} & \frac{\theta_2'(1)}{L} & \dots & \frac{\theta_{11}'(1)}{L} \end{bmatrix}$$

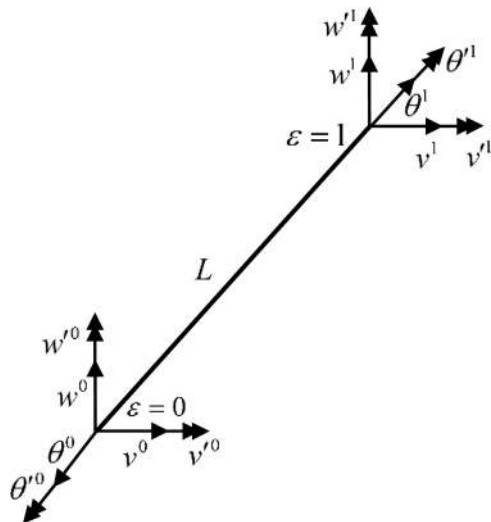


Fig. 2. The nodal displacements of a thin-walled beam.

$$\{D\} = \left\{ v^0 \quad w^0 \quad \theta^0 \quad v^0 \quad w^0 \quad \theta^0 \quad v^1 \quad w^1 \quad \theta^1 \quad v^1 \quad w^1 \quad \theta^1 \right\}^T \quad (36a-b)$$

In the present finite element model, each element has two nodes with six degrees of freedom per node (DOF). The DOF vector of the element is given in Eq. (36b).

From (35), one gets:

$$\{A\} = [V]^{-1}\{D\} \quad (37)$$

Then, the system (33) becomes:

$$\{C(\varepsilon)\} = [B(\varepsilon)][V]^{-1}\{D\} \quad (38)$$

The terms of the element mass and stiffness matrices can be found from the derivatives of the interpolation functions. The shape functions define the deformation shape of the element from applying unit translation, twist, warping or rotation at each of the 12 degrees of freedom, while constraining other eleven nodal displacements as follows

1. $v^0 = 1, w^0 = \theta^0 = v^0 = w^0 = \theta^0 = v^1 = w^1 = \theta^1 = v^1 = w^1 = \theta^1 = 0$
2. $w^0 = 1, v^0 = \theta^0 = v^0 = w^0 = \theta^0 = v^1 = w^1 = \theta^1 = v^1 = w^1 = \theta^1 = 0$
3. $\theta^0 = 1, w^0 = v^0 = v^0 = w^0 = \theta^0 = v^1 = w^1 = \theta^1 = v^1 = w^1 = \theta^1 = 0$
4. $v^0 = 1, v^0 = w^0 = \theta^0 = w^0 = \theta^0 = v^1 = w^1 = \theta^1 = v^1 = w^1 = \theta^1 = 0$
5. $w^0 = 1, v^0 = w^0 = \theta^0 = v^0 = \theta^0 = v^1 = w^1 = \theta^1 = v^1 = w^1 = \theta^1 = 0$
6. $\theta^0 = 1, v^0 = w^0 = \theta^0 = v^0 = w^0 = v^1 = w^1 = \theta^1 = v^1 = w^1 = \theta^1 = 0$
7. $v^1 = 1, v^0 = w^0 = \theta^0 = v^0 = w^0 = \theta^0 = w^1 = \theta^1 = v^1 = w^1 = \theta^1 = 0$
8. $w^1 = 1, v^0 = v^0 = \theta^0 = v^0 = w^0 = \theta^0 = v^1 = \theta^1 = v^1 = w^1 = \theta^1 = 0$
9. $\theta^1 = 1, v^0 = w^0 = v^0 = v^0 = w^0 = \theta^0 = v^1 = w^1 = v^1 = w^1 = \theta^1 = 0$
10. $v^1 = 1, v^0 = v^0 = w^0 = \theta^0 = w^0 = \theta^0 = v^1 = w^1 = \theta^1 = w^1 = \theta^1 = 0$
11. $w^1 = 1, v^0 = v^0 = w^0 = \theta^0 = v^0 = \theta^0 = v^1 = w^1 = \theta^1 = v^1 = \theta^1 = 0$
12. $\theta^1 = 1, v^0 = v^0 = w^0 = \theta^0 = v^0 = w^0 = v^1 = w^1 = \theta^1 = v^1 = w^1 = 0$

(39)

According to these twelve boundary conditions corresponding to each shape function and using Eq. (38), 12 sets of interpolation functions can be derived. These shape functions could be taken any arbitrary shapes which satisfy the boundary conditions of element and internal continuity requirements. Thus the general displacement of the considered beam is related to four shape functions for each displacement parameter:

$$\{C(\varepsilon)\} = \begin{bmatrix} \{N_v\}^T \\ \{N_w\}^T \\ \{N_\theta\}^T \end{bmatrix} \{D\} \quad (40)$$

Where

$$\begin{bmatrix} \{N_v\}^T \\ \{N_w\}^T \\ \{N_\theta\}^T \end{bmatrix} = \begin{bmatrix} N_{v1} & 0 & 0 & N_{v2} & 0 & 0 & N_{v3} & 0 & 0 & N_{v4} & 0 & 0 \\ 0 & N_{w1} & 0 & 0 & N_{w2} & 0 & 0 & N_{w3} & 0 & 0 & N_{w4} & 0 \\ 0 & 0 & N_{\theta1} & 0 & 0 & N_{\theta2} & 0 & 0 & N_{\theta3} & 0 & 0 & N_{\theta4} \end{bmatrix} \quad (41)$$

5. Stiffness and mass matrices

The equilibrium and motion equations have been derived previously in Eqs. (18)–(21) from the principle of minimum potential energy. With the help of the power series method, this system has been used to perform the stability of prismatic and tapered thin-walled beams in both buckling and lateral buckling phenomena [35,36]. In finite element approach the principle of minimum potential energy leads to the following system:

$$([K^*] + [K_G])\{d\} = \{Q\} \quad (42)$$

Where $\{d\}$ and $\{Q\}$ are the displacement and the force vectors. They are related here to beam Degree of Freedom. $[K^*]$ and $[K_G]$ are the elastic and geometrical stiffness matrices. These matrices are carried out by discretization of Eqs. (13) and (14), with the help of the obtained shape functions. In the case of the non-prismatic thin-walled beam, the terms of these matrices are the following:

$$\begin{aligned} [K^*] = & E \int_L \{I_z\{N'_v\}\{N'_v\}^T + I_y\{N'_w\}\{N'_w\}^T \\ & + I_{\phi}\{N'_\theta\}\{N'_\theta\}^T + I_z z_c^2\{N_\theta\}\{N_\theta\}^T + 4I_z z_c^2\{N'_\theta\}\{N'_\theta\}^T \\ & + I_z z_c^2\{N'_v\}\{N_\theta\}^T + \{N_\theta\}\{N'_v\}^T \\ & + 2I_z z_c\{N'_v\}\{N'_\theta\}^T + \{N'_\theta\}\{N'_v\}^T + 2I_z z_c z_c'\{N_\theta\}\{N'_\theta\}^T + \{N'_\theta\}\{N_\theta\}^T \\ & + I_y y_c^2\{N_\theta\}\{N_\theta\}^T + 4I_y y_c^2\{N'_\theta\}\{N'_\theta\}^T \\ & - I_y y_c\{N'_w\}\{N_\theta\}^T + \{N_\theta\}\{N'_w\}^T - 2I_y y_c\{N'_\theta\}\{N'_w\}^T + \{N'_w\}\{N'_\theta\}^T \\ & + 2I_y y_c y_c'\{N_\theta\}\{N'_\theta\}^T + \{N'_\theta\}\{N_\theta\}^T\} \\ & dx + G \int_L J\{N'_\theta\}\{N'_\theta\}^T dx \end{aligned} \quad (43)$$

$$\begin{aligned} [K_G] = & \int_L \{N\{N'_v\}\{N'_v\}^T + \{N'_w\}\{N'_w\}^T + R_c\{N'_\theta\}\{N'_\theta\}^T - z_c z_c'\{N_\theta\}\{N_\theta\}^T \\ & - y_c y_c'\{N_\theta\}\{N_\theta\}^T + z_c\{N'_\theta\}\{N'_v\}^T + \{N'_v\}\{N'_\theta\}^T \\ & + z_c\{N'_v\}\{N_\theta\}^T + \{N_\theta\}\{N'_v\}^T - y_c\{N'_w\}\{N'_\theta\}^T + \{N'_\theta\}\{N'_w\}^T \\ & - y_c\{N'_w\}\{N_\theta\}^T + \{N_\theta\}\{N'_w\}^T - M_z\{N'_w\}\{N'_\theta\}^T + \{N'_\theta\}\{N'_w\}^T \\ & + M_y\{N'_\theta\}\{N'_v\}^T + \{N'_v\}\{N'_\theta\}^T - M'_z\{N'_w\}\{N_\theta\}^T \\ & + \{N_\theta\}\{N'_w\}^T + M'_y\{N'_v\}\{N_\theta\}^T + \{N_\theta\}\{N'_v\}^T \\ & - (M_z y_c + M'_z y_c')\{N_\theta\}\{N_\theta\}^T - (M_y z_c + M'_y z_c')\{N_\theta\}\{N_\theta\}^T \\ & - (\beta_y M_z + \beta_z M_y)\{N'_\theta\}\{N'_\theta\}^T - M_t\{N_\theta\}\{N_\theta\}^T\} dx \end{aligned} \quad (44)$$

where K_{ij}^* is the usual elastic stiffness matrix and $K_{G_{ij}}$ is the geometric stiffness matrix, which accounts for secondary effect of the variable axial force (N) and bending moments (M_y, M_z) on the bending stiffness of the member.

The load vector Q is given by:

$$\begin{aligned} \{Q\} = & \int_L \{p_y\{N_v\} + p_z\{N_w\} - M_{z0}\{N'_v\} - M_{y0}\{N'_w\} \\ & - M_{z0} z_c'\{N_\theta\} - M_{z0} z_c\{N'_\theta\} + M_{y0} y_c'\{N_\theta\} \\ & + M_{y0} y_c\{N'_\theta\} + B_{\omega 0}\{N'_\theta\} + \hat{M}_t\{N_\theta\}\} dx \end{aligned} \quad (45)$$

At this stage, it is important to mention that the elastic and geometric stiffness matrices $[K^*]$ and $[K_G]$ investigated for a tapered beam with arbitrary cross-section can be used to derive the similar stiffness matrices for a beam with uniform cross-section. In this situation, the shear position is constant and the flexural-torsional stiffness matrices are reduced to:

$$\begin{aligned} [K^*] = & E \int_L \{I_z\{N'_v\}\{N'_v\}^T + I_y\{N'_w\}\{N'_w\}^T + I_{\phi}\{N'_\theta\}\{N'_\theta\}^T\} dx \\ & + G \int_L J\{N'_\theta\}\{N'_\theta\}^T dx \end{aligned} \quad (46)$$

$$\begin{aligned} [K_G] = & \int_L \{N\{N'_v\}\{N'_v\}^T + \{N'_w\}\{N'_w\}^T + R_c\{N'_\theta\}\{N'_\theta\}^T + 2z_c\{N'_\theta\}\{N'_v\}^T \\ & - 2y_c\{N'_w\}\{N'_\theta\}^T\} \end{aligned}$$

$$\begin{aligned} & - 2M_z\{N'_w\}\{N'_\theta\}^T + 2M_y\{N'_\theta\}\{N'_v\}^T - 2M'_z\{N'_w\}\{N_\theta\}^T \\ & + 2M'_y\{N'_v\}\{N_\theta\}^T - (\beta_y M_z + \beta_z M_y)\{N'_\theta\}\{N'_\theta\}^T - M_t\{N_\theta\}\{N_\theta\}^T \} dx \end{aligned} \quad (47)$$

In $[K_G]$ matrix, the load eccentricity contribution is present in the last term of (47). These matrices can be easily derived from the linear stability models developed in [8,43,44] where the second variation of the potential energy is employed.

By applying the principle of virtual displacement along the member with distributed mass, the mass matrix terms are derived as:

$$\begin{aligned} [M] = & \rho \omega^2 \int_L \{A\{N_v\}\{N_v\}^T + A\{N_w\}\{N_w\}^T + I_s\{N_\theta\}\{N_\theta\}^T + A z_c\{N_v\}\{N_\theta\}^T \\ & + \{N_\theta\}\{N_v\}^T - A y_c\{N_w\}\{N_\theta\}^T + \{N_\theta\}\{N_w\}^T \\ & + I_{\phi}\{N'_\theta\}\{N'_\theta\}^T + I_z\{N'_v\}\{N'_v\}^T + I_y\{N'_w\}\{N'_w\}^T \\ & + I_z z_c^2\{N_\theta\}\{N_\theta\}^T + I_y y_c^2\{N_\theta\}\{N_\theta\}^T \\ & + z_c I_z\{N'_v\}\{N_\theta\}^T + \{N_\theta\}\{N'_v\}^T - y_c I_y\{N'_w\}\{N_\theta\}^T \\ & + \{N_\theta\}\{N'_w\}^T\} dx \end{aligned} \quad (48)$$

The stiffness and mass matrices of the whole structure can be obtained by assembling each element stiffness and mass matrices according to its nodal displacements. The process of assemblage is described in detail in most stability analysis textbooks [3,4].

The equilibrium Eq. (42) is non-linear, since the stiffness matrix is not constant. The solution is obtained using classical incremental iterative methods. It becomes:

$$([K^*] + [K_G])\{\Delta d\} = \{\Delta F\} \quad (49)$$

In which $\{\Delta d\}$ and $\{\Delta F\}$ are displacements and force increments. In general, the solution is not unique near bifurcation and limit points and an efficient control method must be adopted in the solution of (49). Moreover, near bifurcation points the structure behavior becomes unstable and very sensitive to imperfections. Small perturbations result in large responses. One way to view this is that the stiffness matrix becomes singular when the loads reach the critical values. A study of instability would require suppression of all prebuckling deformation in the analysis and right hand side of the system (49). In linear stability, the geometric stiffness matrix is proportional to the initial stress forces. The buckling loads are obtained from the solutions of the following eigenvalue problem:

$$([K^*] + \lambda[K_G])\{\phi\} = 0 \quad (50)$$

In which λ are the eigenvalues and $\{\phi\}$ are the related eigenvectors. Under compressive loads, they lead to buckling loads and related buckling modes. In the case of lateral stability, one gets the buckling moments and lateral buckling modes.

For free vibration, the problem is similar to Eq. (50), where the mass matrix is put in place of the geometric stiffness matrix. The eigenvalue problem to be solved is:

$$([K^*] - \mu[M])\{\phi\} = 0 \quad (51)$$

Here μ is related the eigenpulsation of the structure ($\mu = \omega^2$) and $\{\phi\}$ is the related eigenmodes of vibration. It is well known that for a system with n degrees of freedom, n buckling modes and n vibration modes are existed, but in practice only the lower ones are of interest in buckling and vibration analyses.

6. Numerical examples

The aim of this section is to demonstrate the accuracy and the validity of the proposed finite element method in the lateral buckling stability and the flexural-torsional buckling analyses of tapered thin-walled beams with arbitrary cross-sections and

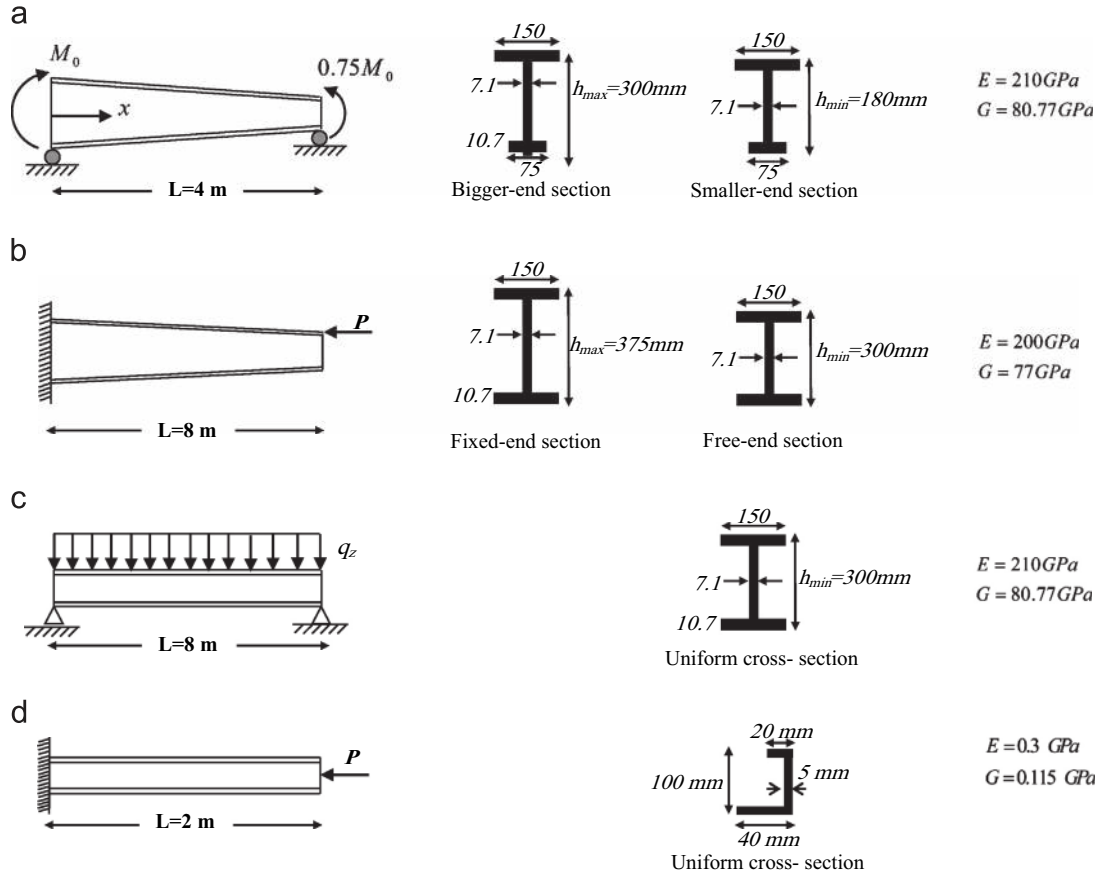


Fig. 3. Cantilevers and simply supported beams with different cross-sections shapes: geometry, loading and material data.

boundary conditions under an eccentrically axial or lateral load and in the free vibration analysis. In order to achieve this goal, some numerical examples are performed. The LTB and FTB loads and natural frequencies provided by the numerical results obtained by aforementioned method are compared to other available analytical or numerical solutions and to finite element method analysis results using ANSYS software [45]. In this code, each studied thin-walled beam is modeled using shell elements (SHELL63). Shell63 has both bending and membrane capabilities. And both in-plane and normal loads are permitted for this element. The element has 6 degrees of freedom at each node, 3 translations in the x , y and z directions and 3 rotations about the 3 axes. In the studied examples, effects of axial and lateral loads eccentrically, the tapering parameter and beam slenderness on FTB and LTB strength are also investigated.

6.1. Example 1

This example has been prepared to verify free vibration and stability analyses of thin-walled members. The present method can be applied for the buckling analysis of various forms of tapered and uniform thin-walled beams with arbitrary cross-section. So to check the accuracy and the validity of proposed method, four cases involving instability analysis of cantilever and simply supported beams with constant cross-sections are presented in this example.

In **Case a**, the buckling moment (M_{cr}) of a simply supported beam subjected to bending moment is investigated (Fig. 3a). This case deals with web tapered thin-walled beam. The web height (the distance between the flange mid-lines) of the beam varies linearly along the length from 300 mm at the right support to 180 mm at the other. The **Case b** is on the estimation of the critical flexural-torsional buckling load of a tapered thin-walled cantilever

beam under a compressive axial load at the top flange of the free end section (Fig. 3b). The web height is made to vary linearly from 375 mm at the fixed-end to 300 mm at the smaller end section. In **Case c**, the lateral stability of a simply supported prismatic beam with doubly symmetric cross-section under lateral uniform distributed load is presented. Table 1 gives the values of the buckling moment ($M_{cr} = q_z L^2 / 8$) of the aforementioned beam when loads are acted at the centroid of the considered I section (Fig. 3c). **Case d** represents the critical buckling load of a prismatic cantilever beam with non-symmetric channel section subjected to an axial compression force on the centroid of the free end section (Fig. 3d).

All the considered thin-walled members and cross-sections are depicted in Fig. 3 with loading, boundary conditions, material properties and geometric dimensions.

Table 1 gives the critical buckling of the tapered and uniform beams with various types of cross-sections. Effect of degree of the power series and number of elements on convergence is also displayed in Table 1. In this table, the critical buckling moments and flexural-torsional buckling loads are carried out from the present finite element method, numerical approach proposed by Asgarian [35] and Soltani [36], finite element method by Kim [15], the analytical solution proposed in [8] and commercial code using Ansys software [45].

As can be seen in Table 1, the satisfactory results for engineering requirements can be reached when the taken number of terms of the power series exceed over 10. Note that in finite element procedure, beam mesh with 4 elements is a good compromise for equivalent accuracy of the accurate buckling loads. In all developed Ansys models in this example, the number of the elements used in the longitudinal direction is selected in each case so that the aspect ratio of the element (length-to-maximum width) is close to unity at the largest cross-section.

6.2. Example 2

This section concerns the flexural–torsional buckling and free vibration analyses of prismatic and web tapered simply supported beams, as shown in Fig. 4. In this example, both analyses are made for two types of cross-section. The first one is a doubly I-section and the second is a singly symmetric I section, with the top flange longer than the bottom flange. In the case of web tapered beam, the top and bottom flanges remain constant along the beam's length while, the web height of the cross-section is varying linearly from (h_{\max}) at the left support to (h_{\min}) at the other support. Thus, the tapering parameter ($\alpha = h_{\min}/h_{\max}$) has been ranged from 0.4 to 1. The compressive axial load is applied at the top flange of the bigger end section. The Beam lengths (L) vary from 6.0 to 12.0 m. The geometrical and the material data are shown in Fig. 4.

Table 2 depicts the elastic buckling loads for the considered simply supported tapered beam illustrated in Fig. 4 which is subjected to constant compressive axial load at the top flange of

Table 1

Effect of number of elements (n) and power series number (N) on linear critical buckling load and natural frequencies of web tapered and prismatic thin-walled beam (Fig. 3a–d).

Case	Number of elements (n)	Present method			References
		Number of terms of power series, N			
		5	10	15	
Case a	1	51.59	69.61	72.5	50.33[45]
	2	50.35	50.89	50.91	49.03 [35]
	3	50.08	50.09	50.09	
	4	49.99	49.93	49.93	
	5	49.96	49.88	49.88	
	6	49.93	49.86	49.86	
	7	49.88	49.85	49.85	
	8	49.86	49.85	49.85	
	9	49.86	49.85	49.85	
Case b	1	43.94	44.03	44.21	43.41 [45]
	2	43.64	43.62	43.73	42.62 [36]
	3	43.62	43.59	43.59	
	4	43.59	43.59	43.59	
	5	43.59	43.59	43.59	
	6	43.59	43.59	43.59	
	7	43.59	43.59	43.59	
	8	43.59	43.59	43.59	
Case c	1	64.7	65.06	65.06	64.66 [8]
	2	64.52	64.54	64.54	63.9 [45]
	3	64.48	64.48	64.48	64.46 [35]
	4	64.47	64.47	64.47	
	5	64.47	64.47	64.47	
Case d	1	16.54	16.54	16.63	14.07 [45]
	2	14.32	14.32	14.38	
	3	13.94	13.94	13.94	13.8 [15,18]
	4	13.93	13.93	13.93	13.93 [36]
	5	13.93	13.93	13.93	

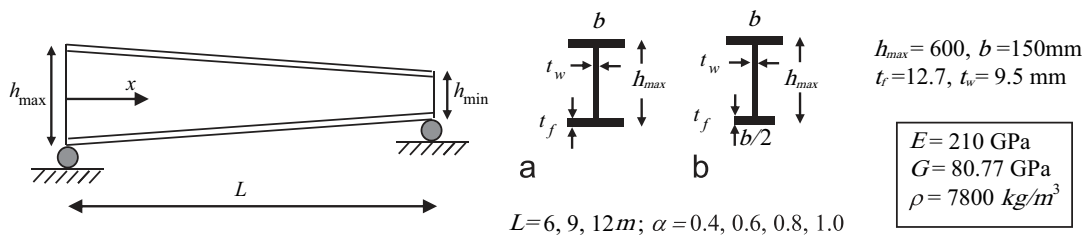


Fig. 4. Simply supported tapered beam under axial compression load: geometry and material properties, (a) doubly symmetric section and (b) singly symmetric section.

the larger cross-section. Also, the lowest values of natural frequency computed for all mentioned cases are shown in Table 3.

In these tables, the obtained results of the described cases in the stability and vibration by the present finite element method based on power series expansions have been compared with those obtained by finite element method using SHELL63 element of Ansys software [45]. Moreover, in the case of stability analysis, a comparison with PSM, investigated by Soltani [36] is made. For more information, the relative errors (Δ) between the present

Table 2

Simply supported tapered beam an axial load at the top flange of the bigger cross-section (Fig. 4): flexural–torsional buckling loads (P_{cr}) and their relative errors (Δ).

L (m)	α	Present method	FTB of simply supported beam (kN), load on top flange						
			Equal flanges			Unequal flanges			
			FEM [45] (Ansys)	Soltani [36]	Δ (%)	Present method	FEM [45] (Ansys)	Soltani [36]	Δ (%)
6	0.4	338.64	343.30	334.326	1.36	231.45	232.98	230.25	0.66
	0.6	345.03	346.58	344.093	0.45	231.44	229.81	229.403	0.71
	0.8	350.61	350.81	353.534	0.06	226.94	229.56	229.18	1.14
	1	358.21	354.93	362.704	0.92	219.60	220.10	217.985	0.23
9	0.4	163.72	164.84	162.641	0.68	103.42	103.65	103.157	0.22
	0.6	165.14	165.58	165.286	0.27	103.49	103.54	102.666	0.05
	0.8	166.19	166.57	167.909	0.23	102.89	103.07	102.5	0.17
	1	168.81	167.54	170.51	0.76	101.77	102.29	101.312	0.51
12	0.4	96.08	96.43	95.764	0.36	58.19	58.27	57.516	0.14
	0.6	96.62	96.72	96.78	0.10	58.23	58.15	57.55	0.14
	0.8	97.05	97.08	97.79	0.03	58.06	57.94	57.577	0.21
	1	97.44	97.42	98.798	0.02	57.61	57.61	57.601	0.00

Table 3

Natural frequencies ω (rad/s) and relative errors (Δ) for simply supported web tapered beam.

L (m)	α	Equal flanges			Unequal flanges		
		Present method	FEM [45] (Ansys)	Δ (%)	Present method	FEM [45] (Ansys)	Δ (%)
6	0.4	43.47	43.12	0.81	30.83	31.82	3.11
	0.6	41.96	41.64	0.77	28.91	29.95	3.47
	0.8	40.6	40.29	0.77	27.04	28.28	4.38
	1	39.35	39.05	0.77	25.23	26.79	5.82
9	0.4	19.31	19.18	0.68	14.83	14.8	0.2
	0.6	18.65	18.52	0.70	14.1	14.08	0.14
	0.8	18.04	17.92	0.67	13.43	13.43	0.00
	1	17.5	17.37	0.75	12.73	12.83	0.78
12	0.4	10.49	10.79	2.78	8.48	8.47	0.12
	0.6	10.87	10.42	4.32	8.11	8.09	0.25
	0.8	10.15	10.08	0.69	7.76	7.75	0.13
	1	9.84	9.77	0.72	7.44	7.44	0.00

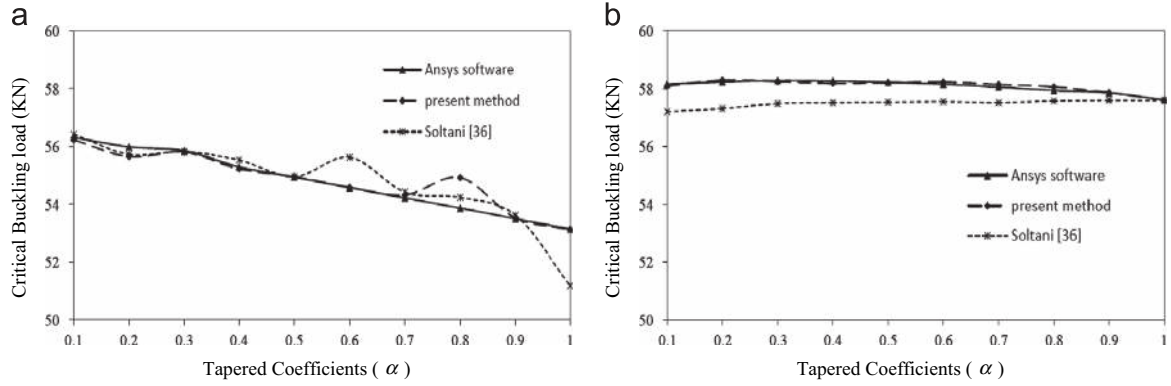


Fig. 5. Variation of the elastic flexural-torsional critical buckling load of the web tapered column ($L=12$ m) versus the tapered parameter (α) in the case the axial load applied at the centroid (a) and on the top flange (b).

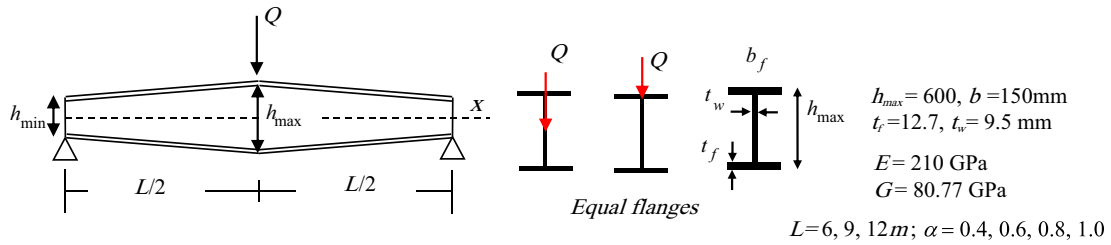


Fig. 6. Simply supported web tapered I-beam under a concentrated load: geometry, material and loading positions.

model and shell predictions of Ansys [45] are also reported in Tables 2 and 3.

The variation of flexural-torsional buckling load of the simply supported web tapered column with singly symmetric cross-section subjected to axial compression load at two different positions (a) on centroid point and (b) on the top flange of the beam depicted in (Fig. 4), versus the tapering coefficient α is illustrated in Fig. 5. For comparison, the same figure shows result obtained by Soltani [36] and Ansys software. As it is seen, results of the present method and Ansys simulations are very close. According to Soltani [36] the results are in good agreement and the difference with finite element simulations is less than 3%.

According to Tables 2 and 3, an excellent agreement is observed with the values of FTB loads and the first natural frequencies derived from this finite element method and the results obtained from numerical analyses and Ansys software.

6.3. Example 3

The third example deals with the lateral-torsional buckling behavior of two sets of doubly symmetric simply supported tapered beams under a concentrated load applied at mid-length, as shown in Fig. 6. In the web tapered beams, the cross-section of top and bottom flanges is usually constant along the length of the beam while, the web height at both supports (h_{min}) is made to reduce by 40%, 50%, 60% and 80% of the highest value (h_{max}). In this example, the tapering coefficient ($\alpha = h_{min}/h_{max}$) has been varied from 0.4 to 1.0. It is also assumed that the beam's geometrical and material parameters are symmetric relative to the x -axis that means the both segments have the same tapering ratio and cross-section. Beam lengths (L) have been varied from 6.0 to 12.0 m. In this example, the buckling loads are carried out for two different load positions: the concentrated lateral load applied at the shear center and on the top flange of mid-span cross-section, as shown in Fig. 6.

In Table 4, the values of Q_{cr} obtained by the proposed FEM based on the expansions of the power series method and finite element results by means of Ansys software [45] are presented. Some other benchmark solutions are also reported: 1D model introduced by Andrade [33] and power series solution investigated by Asgarian [35] for the two load positions and finite element results available in Yang [23] for load position on centroid. The relative errors (Δ) is computed according to $\Delta = (Q_{cr} - Q_{cr}^{FEM}) / Q_{cr}^{FEM} \times 100$.

As shown in Table 4, the values of lateral-torsional buckling loads derived from this method are in good agreement with the numerical results obtained using Ansys code [45] and some other available studies proposed by Yang [23], Asgarian [35] and Andrade [33]. The difference between various solutions is acceptable.

6.4. Example 4

This section concerns the stability and free vibration analyses of two sets of non-prismatic thin-walled beams. In this example, two cross-sections are assumed, a doubly and a singly symmetric I section. In the depicted beam, the flanges' width for both types of cross-sections are made to vary linearly from the fixed end to the tip end. The analyzed beam also exhibits a linear web tapering. The web height is ranging along the beam's length and it is made to reduce to the half at its free end, as shown in Fig. 7. The material data are shown in Fig. 7. The buckling loads are derived when the beam is subjected to a compressive axial load at the top flange of the free end section (point B). Buckling and free vibration analyses are carried out for different beam slendernesses $L=6, 9$ and 12 m.

Tables 5 and 6 represent the flexural-torsional buckling loads and the natural frequencies of the cantilever column with non-uniform cross-section computed by the proposed procedure and compared to those obtained by finite element method using Ansys software [45].

Table 4
Simply supported web tapered I-section under a concentrated load (Fig. 6): linear critical loads comparisons and errors.

L (m)	α	Critical buckling loads (kN)										
		Top flange loading					Centroidal loading					
		Present Study	Q_{cr}^{FEM} Ansys	$Q_{cr}^{Andrade}$ [33]	$Q_{cr}^{Asgarian}$ [35]	$\Delta(\%)$	Present Study	Q_{cr}^{FEM} Ansys	$Q_{cr}^{Andrade}$ [33]	$Q_{cr}^{Asgarian}$ [35]	Q_{cr}^{Yang} [23]	$\Delta(\%)$
6	0.4	61.74	60.05	65.84	59.73	2.81	107.07	100.67	109.75	108.51	109.42	6.36
	0.6	73.35	73.85	72.55	72.81	0.68	120.58	111.50	118.42	122.90	114.04	8.14
	0.8	85.73	83.06	85.07	86.23	3.21	134.73	125.51	133.26	137.23	118.5	7.35
	1.0	98.68	98.78	100.75	99.66	0.10	149.28	139.84	151.28	151.4	151.42	6.75
9	0.4	28.92	29.94	31.03	28.04	3.41	43.75	43.87	45.45	43.95	42.62	0.27
	0.6	32.33	32.23	32.81	31.94	0.31	47.48	46.47	47.55	47.96	44.38	2.17
	0.8	35.88	35.72	36.06	35.89	0.45	51.36	50.21	51.31	51.98	45.95	2.29
	1.0	39.79	39.92	40.24	39.91	0.33	55.38	54.47	55.99	55.99	55.98	1.67
12	0.4	17.12	17.89	18.22	16.703	4.30	23.8	24.22	24.67	24.01	22.67	1.73
	0.6	18.62	18.86	19.03	18.415	1.27	25.36	25.30	25.61	25.53	23.5	0.24
	0.8	20.15	20.26	20.36	20.134	0.54	26.99	26.81	27.10	27.23	27.87	0.67
	1.0	21.83	21.95	22.03	22.047	0.55	28.67	28.57	28.94	28.94	28.92	0.35

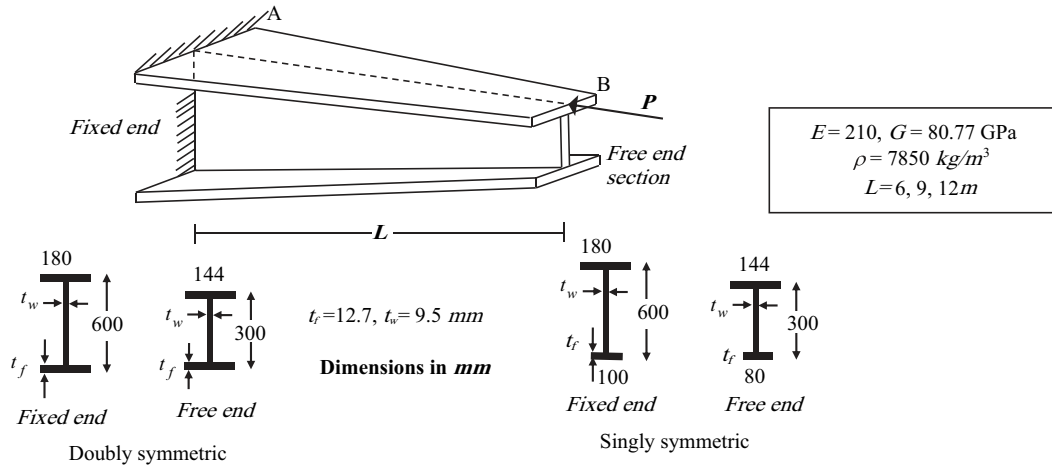


Fig. 7. Tapered I-section cantilever thin-walled beam under axial compressive load: geometry and material properties.

Table 5
Critical buckling load $P_{cr}(kN)$ for the non-prismatic beams with different lengths. (Example 4).

L (m)	Mode number	FTB of a cantilever beam (kN), loaded on top flange					
		Equal flanges			Unequal flanges		
		Present method	FEM [45] (Ansys)	$\Delta(\%)$	Present method	FEM [45] (Ansys)	$\Delta(\%)$
6	1	100.93	99.01	1.94	64.58	64.55	0.05
	2	652.02	633.28	2.96	482.86	448.12	7.75
9	1	47.51	47.52	0.02	29.01	28.92	0.30
	2	312.38	310.84	0.50	225.34	226.40	0.47
12	1	27.49	27.56	0.25	16.38	16.32	0.37
	2	188.03	188.02	0.01	123.66	129.04	4.17

Table 6
The natural frequency $\omega(\text{rad/s})$ for non-prismatic thin-walled beams with doubly or singly symmetric I-section. (Example 4).

L (m)	Mode number	The natural frequency $\omega(\text{rad/s})$					
		Equal flanges			Unequal flanges		
		Present method	FEM [45] (Ansys)	$\Delta(\%)$	Present method	FEM [45] (Ansys)	$\Delta(\%)$
6	1	19.47	19.45	0.07	14.85	15.16	2.04
	2	52.97	51.60	2.66	42.88	42.98	0.23
9	1	8.65	8.65	0.00	6.83	6.87	0.58
	2	29.75	29.71	0.13	24.47	24.46	0.06
12	1	4.87	4.87	0.00	3.91	3.90	0.26
	2	20.23	20.31	0.39	16.42	16.46	0.24

The lowest two critical buckling loads variations with length L for both types of cross-sections are shown in Figs. 8 and 9, for the cantilever non-prismatic beam loaded at the top flange. In the case of the first elastic buckling load, the obtained results by the present finite element method have been compared with those obtained by the closed form solutions using power series expansions [36] and Ansys's shell element [45].

From the comparable cases in example 4 dealing with both free vibration and stability analyses of non-prismatic beams, the

efficiency and sufficiency of the proposed finite element method can be concluded.

6.5. Example 5

In this section, the linear lateral torsional buckling behavior of two sets of thin-walled tapered cantilever beams is addressed. In the first case, the LTB load of doubly symmetric web tapered beam is investigated. In this case, the top and bottom flanges are

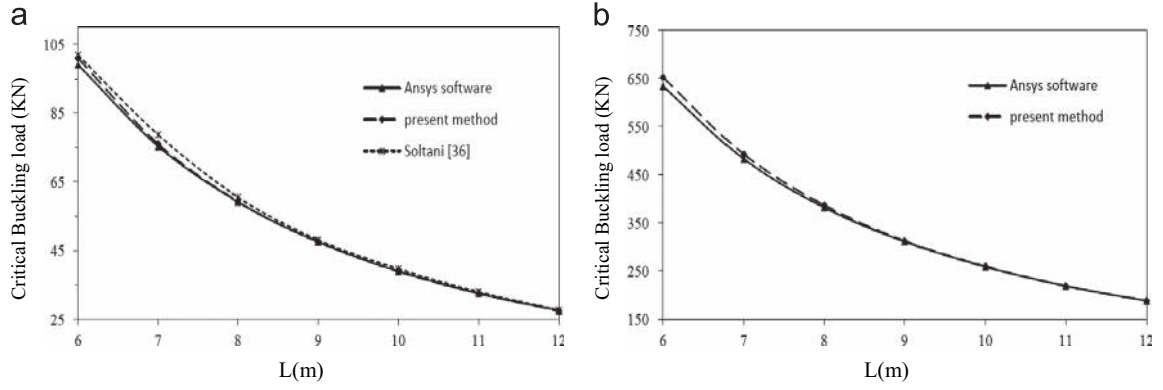


Fig. 8. Critical buckling loads variation versus length L , Equal flanges, (a) the first mode, (b) the second mode.

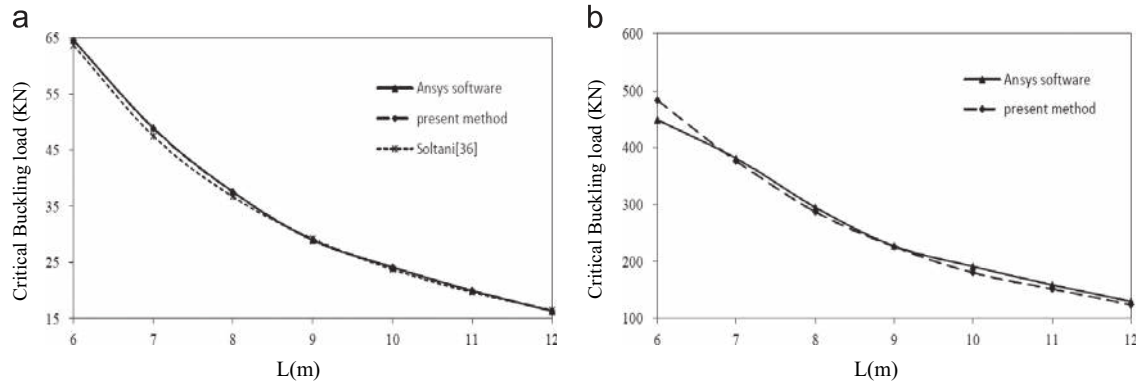


Fig. 9. Critical buckling loads variation versus length L , Unequal flanges, (a) the first mode, (b) the second mode.

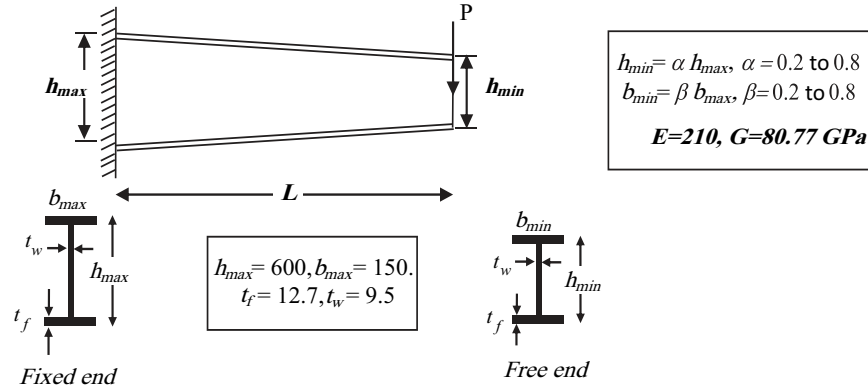


Fig. 10. Tapered I-section cantilever beam: geometry, material and loading properties.

remained constant along the beam's length while, only the web height has been varied linearly from (h_{max}) at the clamped support to (h_{min}) at the free end (Fig. 10). The web height is reduced at the free end with different tapering ratio $\alpha = h_{min}/h_{max}$ ranging from 0.2 to 0.8. In the second case, elastic buckling loads of the flange tapered beam have been carried out. The flange width is varying along the beam length with different relative values of $\beta = b_{min}/b_{max}$ varying from 0.2 to 0.8. For each cantilever beam, a doubly I-section is considered and a concentrated load is applied at the free end, in the cross-section centroid. The analyzed beams exhibit a tapering coefficients α and β ranging from 0.2 to 0.8. The beam lengths (L) have been varied from 6 to 12 m. The material and geometrical properties of the considered beam are shown in Fig. 10.

Table 7 provides the values of the lowest three buckling loads (P_{cr}) computed by the present solution using power series expansions,

those obtained by Ansys software [45], the Rayleigh-Ritz method used in Lei [31] and also the results of the proposed finite element method using 3D beam elements by Ronagh [25,26]. The illustrated beam was modeled using SHELL63 of Ansys [45]. The relative errors (Δ) between the present method and Ansys results are also presented.

An excellent agreement is observed with the values of LTB loads derived from this method and all numerical and analytical aforementioned methods. The difference between the various solutions is within acceptable range.

The variation of the lateral-torsional buckling loads of the web and flange tapered beams with doubly symmetric I-section subjected to lateral load at its shear center point (Fig. 10) versus tapered coefficients are shown in Fig. 11(a)–(b). For comparison, the same figure shows the results obtained by Asgarian [35] and Ansys software. According to Asgarian [35], the results are in good agreement.

Table 7
The elastic critical loads and relative errors for tapered cantilevers with equal flanges (Fig. 10).

L (m)	α or β	Mode number	LTB of cantilever beam (kN)					
			Web tapered			Flange tapered		
			References	Present method	Δ (%)	References	Present method	Δ (%)
8	0.2	1	21.145 [45] 20.95 [31]	20.95	0.92	7.31 [45] 6.5 [25,26]	7.37	0.82
		2	64.31 [45]	62.97	2.08	23.19 [45]	23.42	0.99
		3	122.65 [45]	125.94	2.68	43.66 [45]	45.07	3.23
	0.4	1	21.51 [45] 21.61 [31]	21.56	0.22	10.89 [45] 10.6 [25,26]	11.11	2.02
		2	65.38 [45]	66.82	2.2	34.94 [45]	35.45	1.46
		3	128.89 [45]	136.9	6.21	67.98 [45]	71.29	4.87
	0.6	1	21.75 [45] 22.27 [31]	22.15	1.84	14.63 [45] 14.58 [25,26]	14.98	2.39
		2	66.92 [45]	70.42	5.24	45.93 [45]	48.47	5.53
		3	131.76 [45]	147.09	11.63	90.57 [45]	100.44	10.90
	0.8	1	22.047 [45] 22.92 [31]	22.72	3.05	18.45 [45] 17.93 [25,26]	19.03	3.14
		2	68.32 [45]	73.83	8.07	57.53 [45]	62.36	8.40
		3	134.71 [45]	156.75	16.36	113.96 [45]	132.05	15.87
10	0.2	1	12.33 [45] 12.32 [31]	12.29	0.33	4.43 [45] 3.92 [25,26]	4.46	0.68
		2	36.51 [45]	35.76	2.04	13.73 [45]	13.79	0.44
		3	68.24 [45]	69.42	1.72	25.28 [45]	25.77	1.94
	0.4	1	12.57 [45] 12.67 [31]	12.6	0.17	6.54 [45] 6.08 [25,26]	6.61	1.07
		2	37.32 [45]	37.72	1.07	20.13 [45]	20.42	1.44
		3	72.61 [45]	74.98	3.27	38.41 [45]	39.79	3.59
	0.6	1	12.77 [45] 13.03 [31]	12.91	1.09	8.71 [45] 8.99 [25,26]	8.83	1.38
		2	38.64 [45]	39.62	2.54	26.81 [45]	27.55	2.76
		3	75.864 [45]	80.36	5.93	52.46 [45]	54.98	4.80
	0.8	1	12.98 [45] 13.38 [31]	13.22	1.85	10.93 [45] 10.22 [25,26]	11.12	1.74
		2	39.89 [45]	41.42	3.84	33.75 [45]	35.13	4.09
		3	78.713 [45]	85.3	8.37	66.73 [45]	72.08	8.02

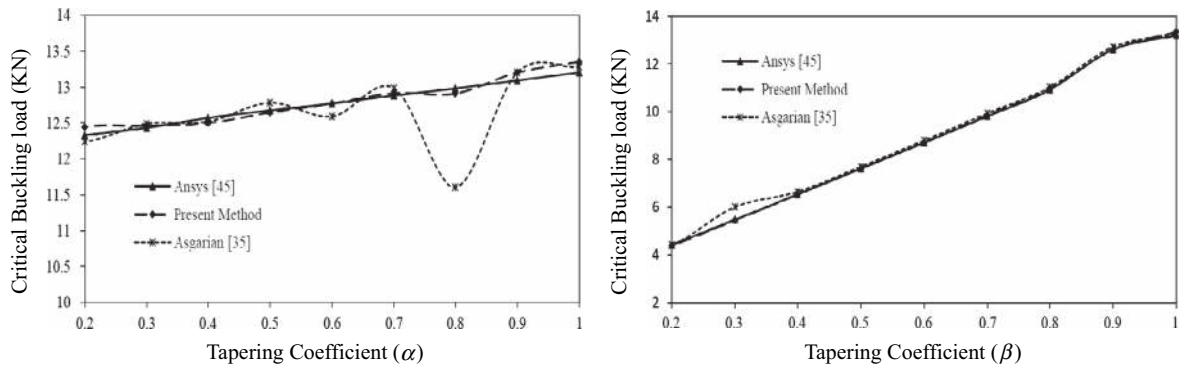


Fig. 11. Variation of the elastic lateral-torsional critical buckling load of the web and flange tapered beam ($L=10$ m) versus tapering ratio (α, β).

6.6. Example 6

The examples in Table 8 are presented to show the accuracy and the exactnesses of presented study to obtain the lowest three natural frequencies of different cases of tapered beams compare to those obtained by Ansys software [45].

Case 1 gives the first three natural frequencies of a web tapered cantilever column under free vibration analysis. The web height is made to vary linearly along the beam length. So the web height is made to reduce into half at the free end of member.

Case 2 denotes a thin-walled cantilever beam with doubly symmetric cross-section. In this case, the web height remains constant along the beam's length but the flange is varying linearly which has a tapering ratio of $b_{\min}/b_{\max} = 0.8$.

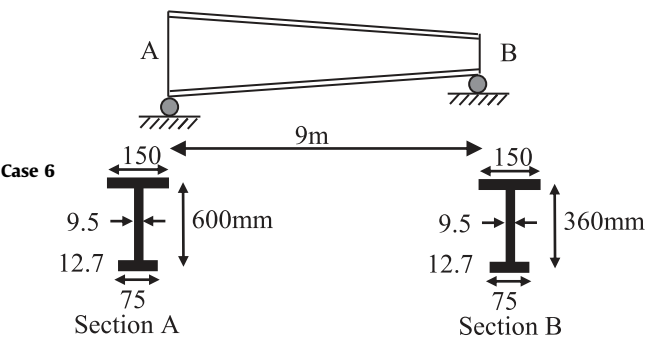
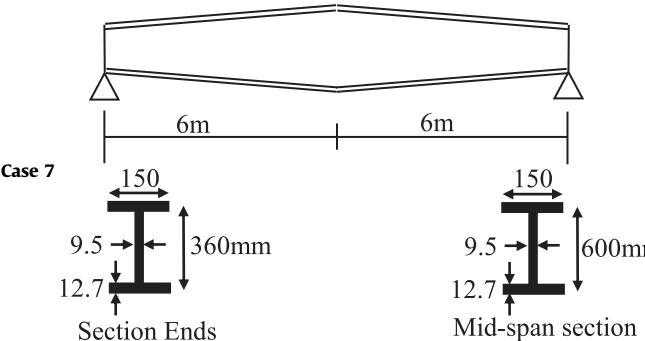
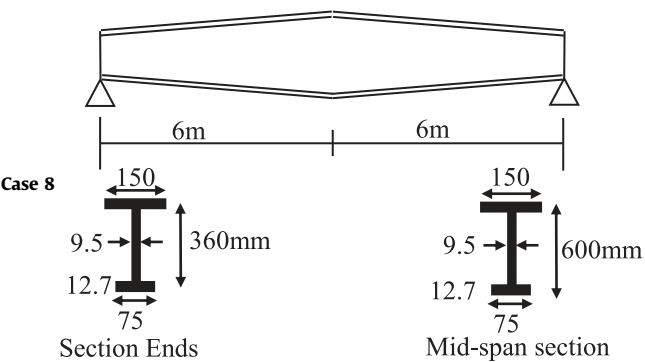
Case 3 signifies the free vibration behavior of a web tapered cantilever with singly symmetric I section. In the case of web tapered beam, the web height of the member varies linearly along the length from 600 mm at the fixed end to 300 mm at the free end.

Case 4 represents the values of natural frequencies of the lowest three vibration modes for the tapered thin-walled beam

Table 8
Effects of tapering and boundary conditions on the lower natural frequencies ω (rad/s) of thin-walled beams.

Data case	Mode number (Type)	FEM [45] (Ansys)	Soltani [36]	Present study
Case 1	1 (Pure bending (v))	11.06	11.12	11.09
	2 (Pure torsion (θ))	33.98	33.98	33.93
	3 (Pure bending (w))	65.001	64.13	65.85
Case 2	1 (Pure bending (v))	9.43	9.5	9.456
	2 (Pure torsion (θ))	21.93	22.06	22.06
	3 (Pure bending (v))	54.56	55.08	54.87
Case 3	1 (Bending-torsional ($v-\theta$))	8.86	9.03	8.68
	2 (Bending-torsional ($v-\theta$))	29.41	29.53	30.87
	3 (Bending-torsional ($v-\theta$))	50.545	49.94	49.98
Case 4	1 (Bending-torsional ($v-\theta$))	7.14	7.62	7.19
	2 (Bending-torsional ($v-\theta$))	19.93	19.05	19.96
	3 (Bending-torsional ($v-\theta$))	37.31	36.28	37.56
Case 5	1 (Pure bending (v))	18.52	18.65	18.65
	2 (Pure torsion (θ))	44.3	43.62	43.63
	3 (Pure bending (v))	73.98	74.71	74.77

Table 8 (continued)

Data case	Mode number (Type)	FEM [45] (Ansys)	Soltani [36]	Present study
 <p>Case 6</p>	1 (Bending-torsional ($v-\theta$))	14.08	14.89	14.12
	2 (Bending-torsional ($v-\theta$))	42.5	41.5	42.56
	3 (Bending-torsional ($v-\theta$))	50.62	48.81	50.8
 <p>Case 7</p>	1 (Pure bending (v))	10.12	10.21	10.21
	2 (Pure torsion (θ))	26.21	26.03	26.05
	3 (Pure bending (v))	41.64	41.95	41.87
 <p>Case 8</p>	1 (Bending-torsional ($v-\theta$))	7.96	8.12	7.52
	2 (Bending-torsional ($v-\theta$))	26.07	25.7	27.57
	3 (Bending-torsional ($v-\theta$))	29.96	30.37	29.75

with singly symmetric I-section. This case deals with flange tapered cantilever. The flange width is varying linearly along the beam's length; therefore, it is made to reduce at the free end, while the web height is remained constant.

Case 5 gives the first three natural frequencies of a simply supported tapered beam under free vibration. The web height is made to vary from bigger end section at the left support to the smaller one at the other.

Case 6 displays the free vibration behavior of a non-prismatic simply supported beam with singly symmetric I section. The beam exhibits a linear web tapering varying from 600 mm at the left support to 360 mm at the other support.

Case 7 concerns the fundamental natural frequencies of a steel simply supported non-prismatic beam with a doubly symmetric I section. The considered beam is composed of two tapered elements, in which the web height is made to increase linearly from 360 mm at the supports to 600 mm in the mid-span while, the top and bottom flanges remain constant along the beam.

Case 8 gives the natural frequencies of a pinned end non-prismatic thin-walled beam with unequal flanges I section under free vibration which was studied in the last case. But

in this case, the mentioned beam has a singly symmetric section.

The geometrical and sectional properties of all cases are shown in (Table 8). For all the study cases, a steel material is assumed. The elastic constants and the mass density are the same as previously.

After observing the results displayed in the Table 8, it can be concluded that there is an excellent agreement between the natural frequencies calculated by present study and those computed by finite element method, using shell element of Ansys software [45] and numerical method based on power series expansions by Soltani [36].

7. Conclusions

In this paper, a numerical model combining the finite element method and the power series expansions is adopted for the buckling stability and free vibration analyses of tapered thin-walled beams with arbitrary cross-sections. The boundary conditions can be arbitrary and effect of load eccentricities has been

taken into consideration. The total potential energy principle considering the effects of strain and initial stress, the kinematic energy and the work of the applied loads is used to derive the equilibrium equations of motion of thin-walled members. Power series expansions method is used to solve the system of fourth order differential equations with variable coefficients and to determine the exact twelve sets shape functions for the non-uniform element with 12 degrees of freedom. In turn, based on the principle of internal virtual work along the element axis, the element stiffness and mass matrices for the buckling and free vibration analyses of non-prismatic thin-walled members are obtained. The proposed method can be applied in various forms of non-prismatic member under axially concentrated loads and variable mass per unit length. Furthermore; it can be used to evaluate both natural frequency and buckling load concurrently.

In order to present the accuracy and efficiency of the proposed computations, some comparable numerical examples are presented and compared with other analytical and numerical solutions. The present model is more efficient and leads to more accurate results. It requires a few elements in mesh process. Furthermore, the method can be applied in prediction of the buckling loads and natural frequencies of uniform members as well as non-prismatic members.

References

- [1] Timoshenko SP, Gere JM. Theory of elastic stability. 2nd ed. New York: McGraw-Hill; 1961.
- [2] Vlasov VZ. Thin-walled elastic beams, Moscow, 1959. French translation, Pièces longues en voiles minces. Paris: Eyrolles; 1962.
- [3] Chen WF, Lui EM. Structural stability, theory and implementation. New York: Elsevier; 1987.
- [4] Bazant ZP, Cedolin L. Stability of structures Elastic, inelastic fracture and damage theories. New York: Dover Publications; 1991.
- [5] Zhang L, Tong GS. Flexural-torsional buckling of thin-walled beam members based on shell buckling theory. Thin-Walled Struct 2004;12:1687–965.
- [6] Zhang L, Tong GS. Elastic flexural-torsional buckling of thin-walled cantilevers. Thin-walled Struct 2008;46:27–37.
- [7] Sapkas A, Kollar LP. Lateral-torsional buckling of composite beams. Int J Solids Struct 2002;39(11):2939–63.
- [8] Mohri F, Brouki A, Roth JC. Theoretical and numerical stability analyses of unrestrained, mono-symmetric thin-walled beams. J Constr Steel Res 2003;59:63–90.
- [9] Andrade A, Camotim D, Providencia P. On the evaluation of elastic critical moments in doubly and singly symmetric I-section cantilevers. J Constr Steel Res 2007;67:894–908.
- [10] Erkmen RE, Mohareb M. Buckling analysis of thin-walled open members- A complementary energy variational principle. Thin-Walled Struct 2008;46: 602–17.
- [11] Erkmen RE, Mohareb M. Buckling analysis of thin-walled open members- A finite element formulation. Thin-Walled Struct 2008;46:618–36.
- [12] Wu L, Mohareb M. Buckling of shear deformable thin-walled members—I. Variational principle and analytical solutions. Thin-Walled Struct 2011;49:197–207.
- [13] Wu L, Mohareb M. Buckling formulation for shear deformable thin-walled members—II Finite element formulation. Thin-Walled Struct 2011;49:208–22.
- [14] Leung AYT. Exact dynamic stiffness for axial-torsional buckling of structural frames. Thin-Walled Struct 2008;46:1–10.
- [15] Kim II N-, Fu CC, Kim M-Y. Stiffness matrices for flexural-torsional/lateral buckling and vibration analysis of thin-walled beam. J Sound Vibr 2007;299:739–56.
- [16] Kim II N-, Lee B-J, Kim M-Y. Exact element static stiffness matrices of shear deformable thin-walled beam-columns. Thin-Walled Struct 2004;42:1231–56.
- [17] Jun L, Wanyou L, Rongying S, Hongxing H. Coupled bending and torsional vibration of non-symmetrical axially loaded thin-walled Bernoulli-Euler beam. Mech Res Commun 2004;31:697–711.
- [18] Mohri F, Damil N, Potier-Ferry M. Large torsion finite element model for thin-walled beams. Comput Struct 2008;86:671–83.
- [19] Mohri F, Damil N, Potier-Ferry M. Theoretical and numerical models for lateral buckling stability of mono symmetric I section beams. Thin-Walled Struct 2010;48:299–315.
- [20] Mohri F, Azrar L, Potier-Ferry M. Vibration analysis of buckled thin-walled elements with open sections. J Sound Vibr 2004;275:434–46.
- [21] Dourakopoulos JA, Sapountzakis EJ. Post buckling analysis of beams of arbitrary cross-section using BEM. Eng Struct 2010;32(11):3713–24.
- [22] Brown TG. Lateral-torsional buckling of tapered I-beams. J Struct Div, ASCE, 107; 1981; 689–97.
- [23] Yang YB, Yau JD. Stability of beams with tapered I-sections. J Eng Mech, ASCE, 113; 1987; 1337–57.
- [24] Pasquino M, Sciarra FM. Buckling of thin-walled beams with open and generally variable section. Comput Struct 1992;44:843–9.
- [25] Ronagh HR, Bradford MA, Attard MM. Non-linear analysis of thin-walled members of variable cross-section. Part I: Theory. Comput Struct 2000;77: 285–99.
- [26] Ronagh HR, Bradford MA, Attard MM. Non-linear analysis of thin-walled members of variable cross-section. Part II: Application. Comput Struct 2000;77:301–13.
- [27] Chen C-N. Dynamic equilibrium of non-prismatic beams defined on an arbitrarily selected co-ordinate system. J Sound Vibr 2000;230(2):241–60.
- [28] Kim S-B, Kim M-Y. Improved formulation for spatial stability and free vibration of thin-walled tapered beams and space frames. Eng Struct 2000;22:446–58.
- [29] Li G-Q, Li J-J. A tapered Timoshenko-Euler beam element for analysis of steel portal frames. J Constr Steel Res 2002;58:1531–44.
- [30] Yau J-D. Stability of tapered I-Beams under torsional moments. Finite Elem Anal Des 2006;42:914–27.
- [31] Lei Z, Shu TG. Lateral buckling of web-tapered I-beams: A new theory. J Constr Steel Res 2008;64:1379–93.
- [32] Andrade A, Camotim D. Lateral-torsional buckling of singly symmetric tapered beams, Theory and applications. J Eng Mech, ASCE, 131; 2005; 586–97.
- [33] Andrade A, Camotim D, Borges Dinis P. Lateral-torsional buckling of singly symmetric web-tapered thin-walled I-beams, 1D model vs. shell FEA. Comput Struct 2007;85:1343–59.
- [34] Andrade A, Providencia P, Camotim D. Elastic lateral-torsional buckling of restrained web-tapered I-beams. Comput Struct 2010;88:1179–96.
- [35] Asgarian B, Soltani M, Mohri F. Lateral-torsional buckling of tapered thin-walled beams with arbitrary cross-sections. Thin-Walled Struct 2013;62: 96–108.
- [36] Soltani M, Asgarian B, Mohri F. Elastic instability and free vibration analyses of tapered thin-walled beams by the power series method. J Constr Steel Res 2014;96:106–26.
- [37] Eisenberger M, Clastornik J. Beams on variable two-parameter elastic foundation. J Eng Mech, ASCE, 113; 1987; 1454–66.
- [38] Eisenberger M. Stiffness matrices for non-prismatic members including transverse shear. Comput Struct 1991;40(4):831–5.
- [39] Eisenberger M. Vibration frequencies for beams on variable one- and two-parameters elastic foundation. J Sound Vibr 1994;176(5):577–84.
- [40] Eisenberger M, Cohen R. Flexural-torsional buckling of variable and open cross-section members. J Eng Mech, ASCE, 121; 1995; 244–54.
- [41] Al-Sadder SZ. Exact expression for stability functions of a general non-prismatic beam-column member. J Constr Steel Res 2004;60:1561–84.
- [42] MATLAB Version 7.6.MathWorks Inc., USA, 2008.
- [43] Achour B, Roberts TM. Nonlinear strains and instability of thin-walled bars. J Constr Steel Res 2000;56:237–52.
- [44] Attard MM. Later Buckling Anal Beams FEM Comput Struct 1986;23:217–31.
- [45] ANSYS, Version 5.4, Swanson Analysis System, Inc., 2007.